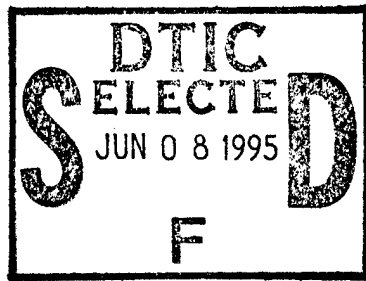# NAVAL POSTGRADUATE SCHOOL
MONTEREY, CALIFORNIA

THESIS

SENSOR DEVELOPMENT FOR
INTELLIGENT PROCESSING OF
AGE HARDENABLE ALUMINUM ALLOYS

by

Robert Andrew Hall Jr.

March 1995

Thesis Advisor: Terry R. McNelley

Approved for public releases; distribution is unlimited.

REPORT DOCUMENTATION PAGE

Form Approved OMB No. 0704-0188

Public reporting burden for this collection of information is estimated to average 1 hour per response, including the time for reviewing instruction, searching existing data sources, gathering and maintaining the data needed, and completing and reviewing the collection of information. Send comments regarding this burden estimate or any other aspect of this collection of information, including suggestions for reducing this burden, to Washington Headquarters Services, Directorate for Information Operations and Reports, 1215 Jefferson Davis Highway, Suite 1204, Arlington, VA 22202-4302, and to the Office of Management and Budget, Paperwork Reduction Project (0704-0188) Washington DC 20503.

1. AGENCY USE ONLY *(Leave blank)*	2. REPORT DATE March 1995	3. REPORT TYPE AND DATES COVERED Master's Thesis

4. TITLE AND SUBTITLE: SENSOR DEVELOPMENT FOR INTELLIGENT PROCESSING OF AGE HARDENABLE ALUMINUM ALLOYS	5. FUNDING NUMBERS
6. AUTHOR(S) Hall, Robert A.	

7. PERFORMING ORGANIZATION NAME(S) AND ADDRESS(ES) Naval Postgraduate School Monterey CA 93943-5000	8. PERFORMING ORGANIZATION REPORT NUMBER

9. SPONSORING/MONITORING AGENCY NAME(S) AND ADDRESS(ES)	10. SPONSORING/MONITORING AGENCY REPORT NUMBER

11. SUPPLEMENTARY NOTES The views expressed in this thesis are those of the author and do not reflect the official policy or position of the Department of Defense or the U.S. Government.

12a. DISTRIBUTION/AVAILABILITY STATEMENT Approved for public release; distribution is unlimited.	12b. DISTRIBUTION CODE

13. ABSTRACT

The objective of this research is to further develop a sensor system which can be used to continuously monitor the aging response of heat treatable aluminum alloys. This type of system would allow for "real time" evaluation of alloy properties as the material is age hardened. Such continuous monitoring, coupled with a control system, is referred to as "intelligent processing". The system consists of eddy current coils incorporated in an impedance bridge circuit, this allows for continuous monitoring of the resistivity difference between a pure aluminum reference sample and the aluminum alloy as it age hardens. This resistivity change is a measure of the change in the alloys microstructure. This system will allow for active control over the final product of an alloy subjected to single- or multi-stage heat treatment thus leading to a higher reliability of engineering structures.

14. SUBJECT TERMS Aging response, Continuous measurement, Aluminum alloys, Eddy current methods, Intelligent processing, Heat treating			15. NUMBER OF PAGES 76
			16. PRICE CODE

17. SECURITY CLASSIFICATION OF REPORT Unclassified	18. SECURITY CLASSIFICATION OF THIS PAGE Unclassified	19. SECURITY CLASSIFICATION OF ABSTRACT Unclassified	20. LIMITATION OF ABSTRACT UL

NSN 7540-01-280-5500

Standard Form 298 (Rev. 2-89)
Prescribed by ANSI Std. 239-18 298-102

i

SENSOR DEVELOPMENT FOR
INTELLIGENT PROCESSING OF
AGE HARDENABLE ALUMINUM ALLOYS

by

Robert A. Hall Jr.
Lieutenant, United States Navy
B.S., Massachusetts Maritime Academy, 1984

Submitted in partial fulfillment
of the requirements for the degree of

MASTER OF SCIENCE IN MECHANICAL ENGINEERING

from the

NAVAL POSTGRADUATE SCHOOL
March 1995

Author: _____
Robert A. Hall Jr.

Approved by: _____
Terry R. McNelley, Thesis Advisor

_____
Matthew D. Kelleher, Chairman
Department of Mechanical Engineering

ABSTRACT

The objective of this research is to further develop a sensor system which can be used to continuously monitor the aging response of heat treatable aluminum alloys. This type of system would allow for "real time" evaluation of alloy properties as the material is age hardened. Such continuous monitoring, coupled with a control system, is referred to as "intelligent processing". The system consists of eddy current coils incorporated in an impedance bridge circuit, this allows continuous monitoring of the resistivity difference between a pure aluminum reference sample and the aluminum alloy as it age hardens. This resistivity change is a measure of the change in the alloys microstructure. This system will allow for active control over the final product of an alloy subjected to single or multi-stage heat treatment thus leading to a higher reliability of engineering structures.

TABLE OF CONTENTS

ACKNOWLEDGMENTS

First of all I would like to thank my thesis advisor, Professor Terry McNelley, for allowing me to undertake this project. His continuous support and guidance throughout the past six months has kept me on track and continually moving forward.

A special thanks to Tom McCord, Tom Christian and the Naval Postgraduate machine shop whose technical support and expeditious service helped to make my job so much easier.

An acknowledgment and appreciation goes out to the Naval Air Warfare Center, with Dr. William Frazier as program monitor, for continued support of the intelligent processing concept.

Finally, and most importantly, I want to thank God for giving me such a loving and supportive wife, Kasey, and two beautiful children, Andrew and Rebecca. They could never know how much there love, and smiles carried me through even the longest days.

I. INTRODUCTION

The objective of this research was to improve a sensor system originally designed by Esarey [Ref. 1] and subsequently modified by Mata [Ref. 2]. The sensor system is intended to be used to continuously monitor, in real time, the age hardening of aluminum alloys.

Strengthening of an aluminum alloy by precipitation heat treatment is essentially a three-step process. First, the material is solution heat treated for a predetermined time and temperature. This step is designed to dissolve the soluble phases in order to get a single-phase structure. Next, the material is quickly quenched to room temperature, which traps and retains solute atoms and excess vacancies in solution, and results in an unstable, supersaturated condition. Finally, during the aging process the material is reheated to a specified temperature, below the solvus, for a specified length of time. This reheating allows solute atoms to diffuse and form a second-phase dispersion. These dispersions evolve following a precipitation sequence characteristic of the material being treated.

Precipitation, or age, hardening of aluminum alloys is currently being accomplished using times and temperatures empirically proven to give a desired combination of mechanical, electrical, corrosion and other properties. This 'cook book' approach does not take into account material variability due to factors such as composition, grain size, degree of cold work, or quench rate from solution heat treatment. These all affect the final outcome of the precipitation heat treatment process. Heat treaters must wait until completion to determine the success or failure of the aging operation. This determination is accomplished by destructive or non-destructive testing such as hardness testing or resistivity measurement. Currently, resistivity testing is a non-destructive post-heat-treatment method of determining the state of aging obtained.

Esarey [Ref. 1] examined the possibility of employing existing eddy current resistivity measuring equipment, coupled with a data acquisition computer, to monitor the progress of aging in real time. This computer assisted, real time approach, known as

1

"intelligent processing" [Ref. 3], would allow for greater control over the heat treatment process by terminating the operation when desired properties are obtained, as indicated by the change in the materials resistivity. The broad range of specifications for heat treated material could be narrowed and this would ultimately lead to higher performance, greater reliability, and greater service life of engineering structures as well as savings in time and money.

Esarey [Ref. 1] , with modifications by Mata [Ref. 2], devised a monitoring system which was capable of measuring a relative resistivity change in real time during the aging process of an alloy sample. This change in resistivity was then correlated with mechanical test data to accurately reflect the evolution of mechanical properties during the aging process. The system consists of the following components:

1) Two spiral-wound sensor probes mounted in a testing frame;

2) A bridge carrier/amplifier which includes an oscillator, impedance bridge circuit, phase sensitive demodulator, and a signal amplifier/filter;

3) A Hewlett Packard 3478A digital multimeter;

4) An IBM compatible PC (with a DT2801 series data acquisition board to collect time and voltage data for subsequent analysis);

5) Two K-type thermocouples;

Applying the above equipment, time and impedance bridge unbalance (r.m.s.) voltage data files were obtained. Plots of aging time versus voltage were generated for various aging processes. These plots revealed consistent behavior, namely, an initial increase in resistivity to a maximum followed by a subsequent decrease. The rates of increase and decrease in resistivity were greater as the aging temperature increased. This was interpreted as representing the increased rate of diffusion and/or precipitation characteristic of higher aging temperatures. Mata [Ref. 2] performed mechanical testing on Al 7075 samples aged for various times at the -T6 tempering temperature of 120 ^{0}C. The hardness, ultimate strength, and yield strengths each progressively increased with aging time, while the percent elongation decreased. These results indicated that the

mechanical properties and bridge unbalance voltage data could be utilized in a system to control heat treating operations.

The following chapters will develop further the background on this subject, present further modifications and improvements to the apparatus, and describe in more detail the different portions of the time versus voltage plots obtained by this system.

II. BACKGROUND

A. ELECTRICAL RESISTIVITY

The electrical resistivity of a metallic material is dependent on many factors. Imperfections in the crystal lattice, including solute impurities, dislocations, precipitates and thermally induced vibration of atoms all influence the resistivity of a metal. A basic understanding of resistivity and the factors which influence it is a necessary prerequisite to understanding how the induced eddy currents in the sensor system are used to evaluate the extent of aging. A more detailed explanation of resistivity in metals can be found in References 4-6. In Reference 7 resistivity is defined as a measure of a material's resistance to the passage of electric current. All materials have a characteristic resistance which is often given as a percent of the International Annealed Copper Standard (IACS). In this system, the resistance of an unalloyed, annealed copper standard is arbitrarily rated at 100% and all other metals and alloys are compared to this standard. Table 2.1 list some common metals and alloys with their respective IACS values.

Metal or alloy	Resistivity, $\mu\Omega \cdot mm$	Conductivity, % IACS
Silver	16.3	105
Copper, annealed	17.2	100
Gold	24.4	70
Aluminum	28.2	61
Aluminum alloys		
6061-T6	41	42
7075-T6	53	32
2024-T4	52	30
Magnesium . . . .'.	46	37
70-30 brass	62	28
Phosphor bronzes	160	11
Monel.	482	3.6
Zirconium	500	3.4
Zircaloy-2	720	2.4
Titanium	548	3.1

Table 2.1 Electrical Resistivity And Conductivity of Several Common Metals and Alloys. From Ref. [8].

Aluminum alloys and metals in general have relatively low resistivity due to the large number of free electrons (charge carriers) which exist in metallically bonded substances. In metallic materials, valence electrons (i.e. electrons in the outermost electron shell) are not bound to any particular atom in the solid. These wave-like free electrons occupy a band of closely spaced energy levels and are able to absorb energy in small quanta. For this reason, they are virtually free within the material [Ref. 6] and can be thought of as charge-carrying particles in random, unbiased motion. When an electric field is applied this motion becomes biased in a direction opposite to the applied field (Figure 2.1). Besides the number of free electrons the resistivity is also a function of the ease in which they can move within the metal. Scattering of these free electrons by crystalline defects creates an increase in resistivity. This scattering phenomenon may be explained in terms of the electron mobility, μ_e (cm^2/(V-sec)), and drift velocity, v_d (cm/sec). Mobility is a measure of the frequency of scattering events and drift velocity is the average electron velocity in the direction of the force imposed by an applied electric field (ε); thus

$$v_d = \mu_e \, \varepsilon \qquad (2.1)$$

A schematic diagram showing the effect of scattering events on the path of a free electron is shown in Figure 2.1. The drift velocity is simply the net electron motion divided by the time to travel that distance. The resistivity, ρ, of a material is given by:

$$\rho \equiv \frac{1}{\mu_e n q} \qquad (2.2)$$

Where μ_e is the mobility, n is the number of conduction electrons, and q is the charge on each electron. More closely spaced scattering events would decrease the mobility of the free electrons which, in turn, creates an increase in the resistivity. Such change in

6

scattering events and the associated changes in resistivity of an aluminum alloy is the essential concept exploited in the eddy current sensor system.
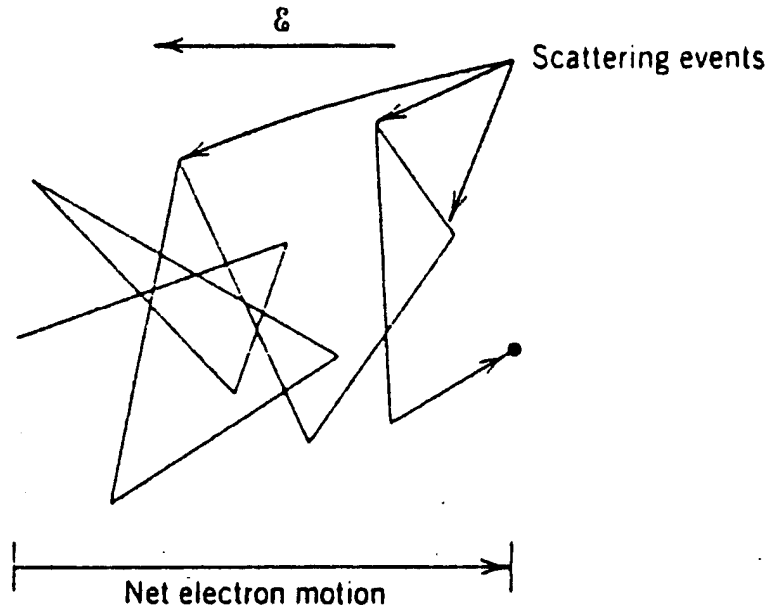

Figure 2.1 Schematic diagram showing the path of an electron that is deflected by scattering events. From Ref. [7].

B. EFFECTS OF TEMPERATURE, SOLUTES, AND PLASTIC DEFORMATION ON RESISTIVITY

As noted earlier, temperature, solute content, and plastic deformation all play an important role in the resistivity of a material. The total resistivity can be represented mathematically as the linear sum of all these contributions. This is Matthiessen's rule [Ref. 8]:

$$\rho = \rho_t + \rho_i + \rho_d \qquad (2.3)$$

where ρ_t, ρ_i, and ρ_d represent the individual contributions of temperature, solute inclusions, and plastic deformation respectively. This is shown graphically in Figure 2.2.
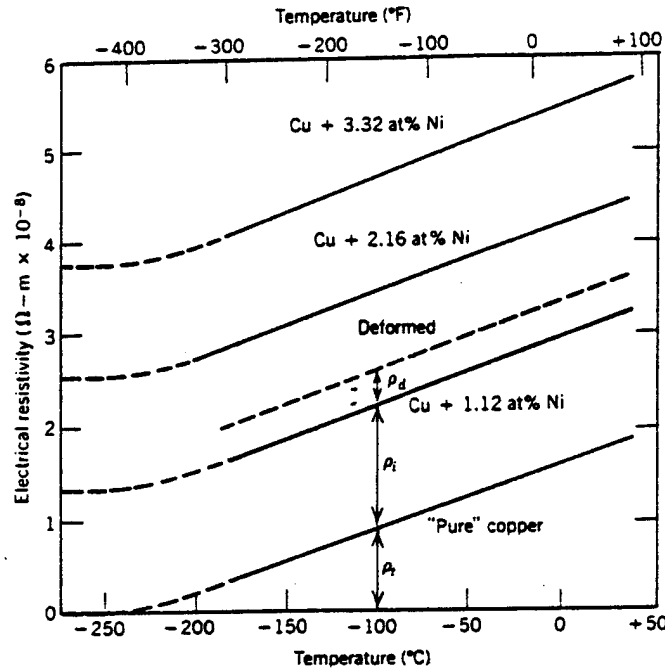

Figure 2.2. The electrical resistivity versus temperature for copper and three copper-nickel alloys, one of which has been deformed. Thermal, impurity, and deformation contributions to the resistivity are indicated at -100° C. From Ref. [7].

1. Temperature Effects

The temperature dependence of resistivity is approximately linear over a wide range of temperatures for most metals, as indicated in Figure 2.2. Thus

$$\rho = \rho_o + \rho_o \, \alpha \, (T - T_o) \qquad (2.4)$$

where ρ_o is the resistivity at the reference temperature T_o, and α is a constant characteristic of the material and known as the thermal coefficient of resistivity. For pure aluminum the value of α is 4.4×10^{-3} K^{-1}. Values for resistivity and thermal coefficients of

resistivity for other common metals are given in Table 2.2. As the temperature of a metal is increased, free electrons are increasingly scattered due to thermally induced atom displacements. That is, the mean free path of the electron is becoming shorter due to the increased oscillations of the atoms. This is presented graphically in Figure 2.3 (a&b). On the other hand, as the temperature of a pure, annealed metal approaches absolute zero, the resistivity also approaches zero. Besides thermal vibration of atoms, temperature plays another important role in the change of resistivity of metal alloys which will be discussed in section 2.B.3.

Material	Resistivity ρ $\Omega \cdot m$	Temperature coefficient of resistivity $\alpha \ K^{-1}$
Typical Metals		
Silver	1.62×10^{-8}	4.1×10^{-3}
Copper	1.69×10^{-8}	4.3×10^{-3}
Aluminum	2.75×10^{-8}	4.4×10^{-3}
Tungsten	5.25×10^{-8}	4.5×10^{-3}
Iron	9.68×10^{-8}	6.5×10^{-3}
Platinum	$10.6 \ \times 10^{-8}$	3.9×10^{-3}
Manganin[a]	$48.2 \ \times 10^{-8}$	0.002×10^{-3}

Table 2.2 Resistivities of Some Materials at Room Temperature. From Ref. [9]

2. Resistivity Changes Due to Solutes

Both substitutional and interstitial solute atoms, as well as vacancies, combine to increase the resistivity of a metal. These impurities increase the number of scattering events which, in turn, corresponds to a lower electron mobility and thus a higher resistivity. As shown in Figure 2.3 (c), the mean free path between scattering events is reduced considerably by the addition of alloying elements. This increase in resistivity is

especially pronounced when the solutes are in solution. Thus, a fully solutionized sample
will be near its peak resistance. Table 2.3 shows the average resistivity increase in
aluminum for various solute atoms, both in and out of solution. This decrease in
resistivity when a trapped solute diffuses and precipitates, out of solution will be discussed
in more detail in the following section.

Element	Maximum solubility In Al, %	Average Increase In resistivity per wt%, $\mu\Omega \cdot cm$	
		In solution	Out of solution(a)
Chromium	0.77	4.00	0.18
Copper	5.65	0.344	0.030
Iron	0.052	2.56	0.058
Lithium	4.0	3.31	0.68
Magnesium	14.9	0.54(b)	0.22(b)
Manganese	1.82	2.94	0.34
Nickel	0.05	0.81	0.061
Silicon	1.65	1.02	0.088
Titanium	1.0	2.88	0.12
Vanadium	0.5	3.58	0.28
Zinc	82.8	0.094(c)	0.023(c)
Zirconium	0.28	1.74	0.044

Note: Add above increase to the base resistivity for high-purity aluminum, 2.65 $\mu\Omega \cdot cm$ at 20 °C
(68 °F) or 2.71 $\mu\Omega \cdot cm$ at 25 °C (77 °F).
(a) Limited to about twice the concentration given for the maximum solid solubility, except as noted.
(b) Limited to approximately 10%. (c) Limited to approximately 20%.
Source: L.A. Willey. Alcoa Research Laboratories.

**Table 2.3 Effect of Elements In and Out of Solid Solution on the Resistivity of
Aluminum. From Ref. [16].**

3. Effect of Precipitation on Resistivity

In the simplest heat treatment operation, e.g. annealing, the temperature is held at
a constant value for a specified amount of time. As seen in Figure 2.2, for any given
temperature there is a corresponding resistivity, depending on the alloying element content
and the degree of deformation. However, for a material which undergoes a precipitation
reaction during annealing, the resistance is not only a function of temperature but also of
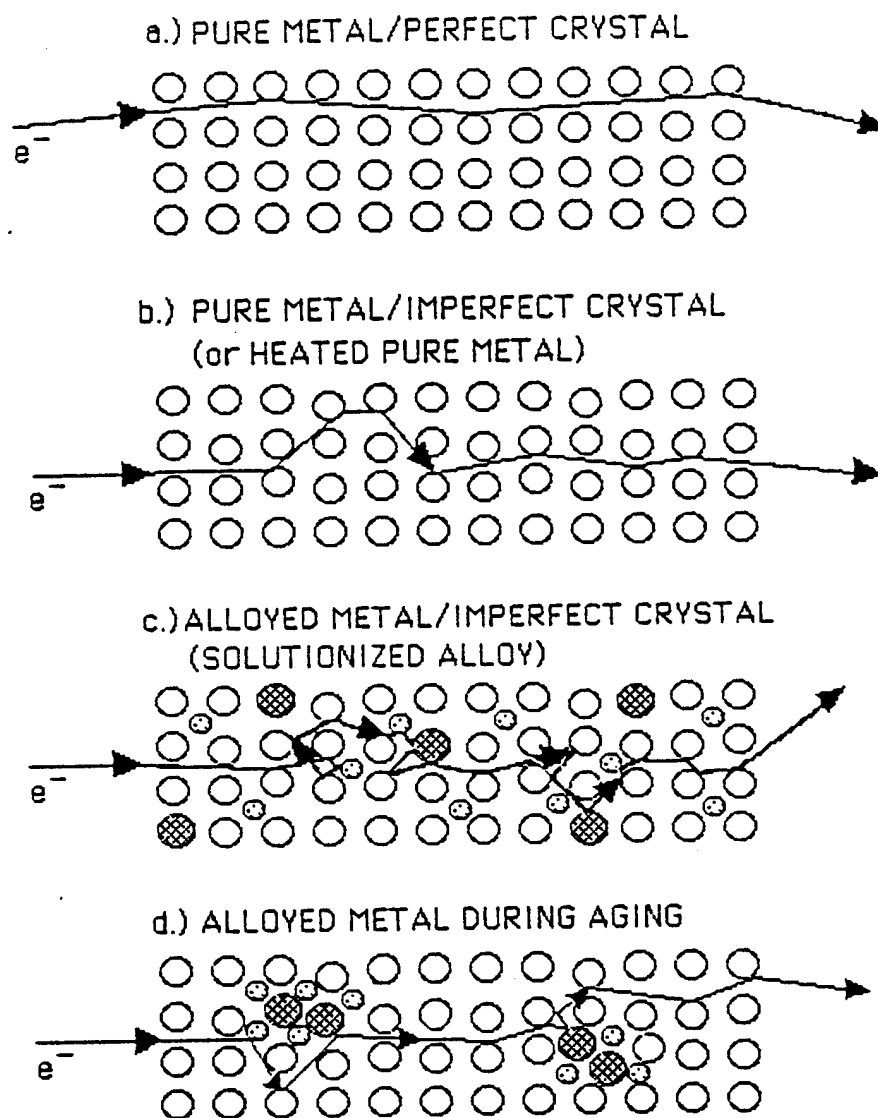time. As such a precipitation-hardenable material ages, the trapped solute atoms begin to

a.) PURE METAL/PERFECT CRYSTAL

b.) PURE METAL/IMPERFECT CRYSTAL
(or HEATED PURE METAL)

c.) ALLOYED METAL/IMPERFECT CRYSTAL
(SOLUTIONIZED ALLOY)

d.) ALLOYED METAL DURING AGING

Figure 2.3   Simplified resistivity models.   From Ref. [1].

11

cluster by diffusion to create Guinier-Preston (G.P.) zones. At first, the strain field around these zones will scatter electrons and create an initial increase in resistivity. A widely accepted theory is that the maximum resistivity obtained corresponds to a critical size of G.P. zones equal to the wavelength of the conduction electrons [Ref.10]. As The G.P. zones continue to grow and transform into precipitates, the remaining solute content in solution is reduced enough to provide a more unobstructed path which offsets the effects of the strain field (Fig. 2.3(d)). Thus, resistivity decreases as growth continues. In this case Matthiessen's rule can be written as (neglecting dislocation effects);

$$\rho(T,t) = \rho_t(T) + \rho_i(t) \tag{2.5}$$

where T is the temperature of the material, and t is the time spent at that temperature. The primary goal of the eddy current sensor system is to be able to continuously monitor and then correlate this changing resistance to the resultant mechanical properties.

4. Resistivity Changes Due to Plastic Deformation

The increased number of dislocations associated with plastic deformation is another source of electron scattering. This scattering occurs because of the strain fields surrounding the dislocation which impede the electrons. Increasing the number of these dislocations subsequently decreases the mean free path of the electrons and resistivity is increased. In the present work, specimens which had undergone plastic deformation were not tested. However, the effect on resistivity by dislocations also decreases with time and temperature. As the temperature is increased, the dislocations become able to move within the material and tend to take up positions of minimum energy [Ref. 6]. With time these dislocations begin to diminish in number due to absorption into dislocation sinks, e.g. grain boundaries, or through mutual annihilation. This effect would have to be considered when monitoring the heat treatment of previously cold worked material.

C. EDDY CURRENT INSPECTION

1. Eddy Current Theory

Eddy current inspection methods are currently being used to identify a wide variety of physical and mechanical conditions in electrically-conductive, ferromagnetic and non-ferromagnetic metals [Ref. 8]. This technique is based on the principles of electromagnetic induction and does not require direct electrical contact with the specimen being examined. Thus, eddy current testing is a non-destructive method of inspection. References 8 and 11-14 provide further, more detailed analysis of the theory and use of eddy current methods. The present discussion will be limited to the use of eddy currents as a tool to determine resistivity in age-hardenable alloys.

When a specimen is to be inspected using eddy current methods, it is placed within or adjacent to an electric coil in which an alternating (or exciting) current is flowing. As shown in Figure 2.4, this current causes eddy currents to flow in the specimen as a result of electromagnetic induction. These induced eddy currents are opposite in polarity to the current flowing within the coil wires and create a back electromotive force (Emf) which increases the impedance of the coils. The magnitude of these currents depends on the primary field established by the alternating current, the electrical characteristics of the specimen, and the electromagnetic fields set up by currents flowing within the part [Ref. 8]. Since the alternating current employed in this work is constant, and the age hardenable alloys inspected are paramagnetic (i.e., have a magnetic permeability very close to 1.0), the primary variable exploited will be the change in the material's electrical characteristics. When the resistivity of a specimen decreases, the magnitude of the induced eddy currents increases. This corresponds to an increase in the back Emf and increased probe coil impedance [Ref. 1]. Two probe coils, each connected to separate legs of an impedance bridge network, can be used in what is known as an "absolute coil arrangement". In this arrangement, a reference sample (pure aluminum in this work) is placed over one probe while the sample being tested (i.e., Al 7075 alloy) is placed over the
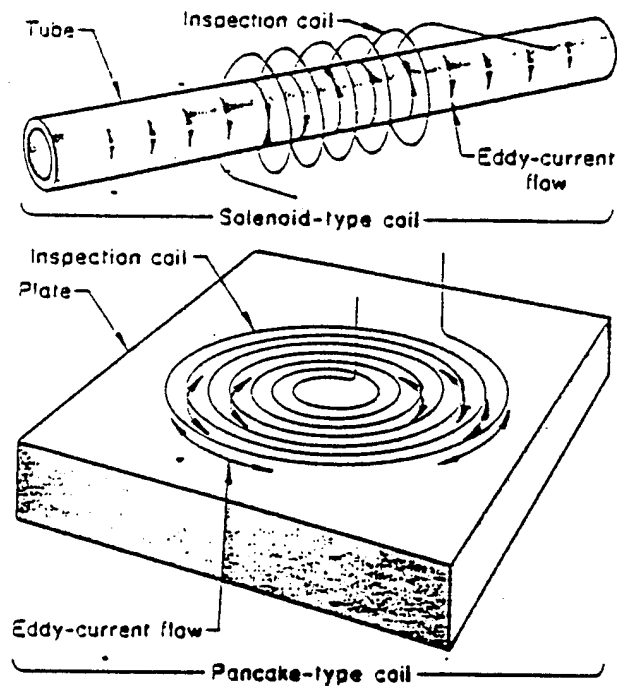
Figure 2.4 Two types of common inspection coils and the pattern of eddy current flow generated by the exciting current in the coils. From Ref. [8].

other.   In this set up, one coil is able to detect the change in resistivity during the aging cycle while the other monitors the constant resistivity of the standard. The difference between the two creates a bridge unbalance voltage which changes as aging progresses. This method of eddy current testing is based solely on indirect measurement, and a correlation between the bridge output and mechanical properties, for each material type and heat treatment process, must be established.

2. Additional Eddy Current Operating Variables

There are basically seven principle operating variables encountered in eddy current testing. Coil impedance, electrical conductivity/resistivity and magnetic permeability have already been mentioned. The remaining variables are lift-off and fill factors, edge effects and skin effects. Fill factors come into effect only when using encircling coils which are not relevant to the present work and will not be discussed here.

a. Lift-off Factor

The relative proximity of the coil to the sample plays a major role in the magnitude of the induced eddy currents. Any variation from full contact will result in what is known as "lift-off" effects. Small coils are especially sensitive to these variations. In the impedance bridge circuit used in this work, lift-off reduces the magnitude of the induced eddy currents in the sample which decreases the back Emf on the coil. This creates a decreased probe coil impedance and a higher unbalance voltage. The effect on BCA voltage output due to sample lift-off is shown in Fig. 4.11. To maintain sample to sample consistency of the magnitude of induced eddy currents it is necessary to maintain a constant relationship between the size and shape of the coils and the size and shape of the part being inspected [Ref. 8].

b. Edge Effects

Whenever an inspection coil is placed too close to an edge of the sample being tested, the eddy currents are unable to flow freely and become distorted. This distortion is known as "edge effect". According to Ref. 8, it is inadvisable to inspect any closer than 0.12 inch (3.0 mm) from any edge. In the apparatus designed by Mata [Ref. 2], each sample is positioned on top of a coil with a minimum of 0.25 inch (6.0 mm) distance to each edge in order to eliminate this effect.

c. Skin Effects

The induced eddy currents are always most dense at the surface in contact with the coils and progressively diminish with depth into the sample. Figure 2.5 shows the variation in density of induced eddy currents as a function of depth below the surface. The depth at which the density of the eddy currents is reduced to 37 % of the surface value is known as the "standard depth of penetration" and may be determined by the following equation:

$$S = 1980\sqrt{\frac{\rho}{\mu f}}$$ (2.6)

where S is the standard depth of penetration (inches), ρ is the electrical resistivity (ohm-cm), μ is the magnetic permeability (1.0 for non-magnetic materials), and f is the inspection frequency (hertz). As can be seen, any increase in resistivity or decrease in the inspection frequency would result in an increase of the depth of penetration. Figure 2.6 shows for the frequency of 52 KHz used in these experiments, a depth of penetration of 0.02 inches (0.5 mm) is obtained in the pure aluminum reference sample. A larger depth is obtained in the Al 7075 alloy because of the increased resistance. It has been found that mechanical and physical properties of the bulk are well represented just 20 μm below the specimen surface [Ref. 14]. Since eddy currents are present beyond the standard depth, it is advised that the sample be at least two or three times thicker than this depth to avoid any significant effect on the eddy current response [Ref. 8].
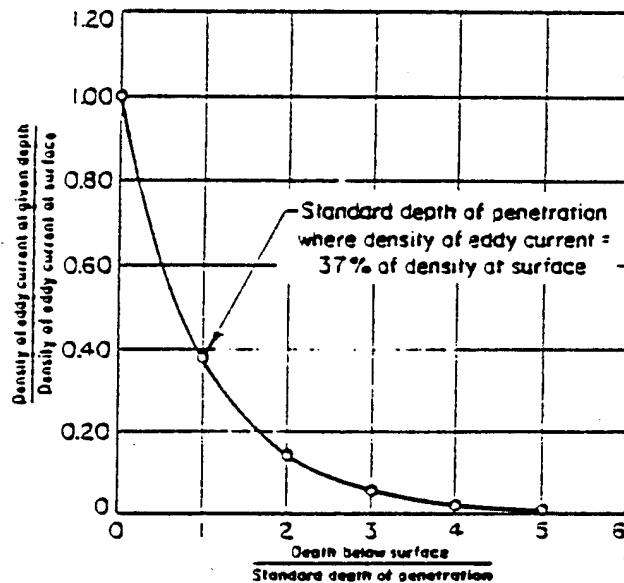

Figure 2.5   Variation in density of eddy currents as a function of depth below the surface of a conductor. From Ref. [8].
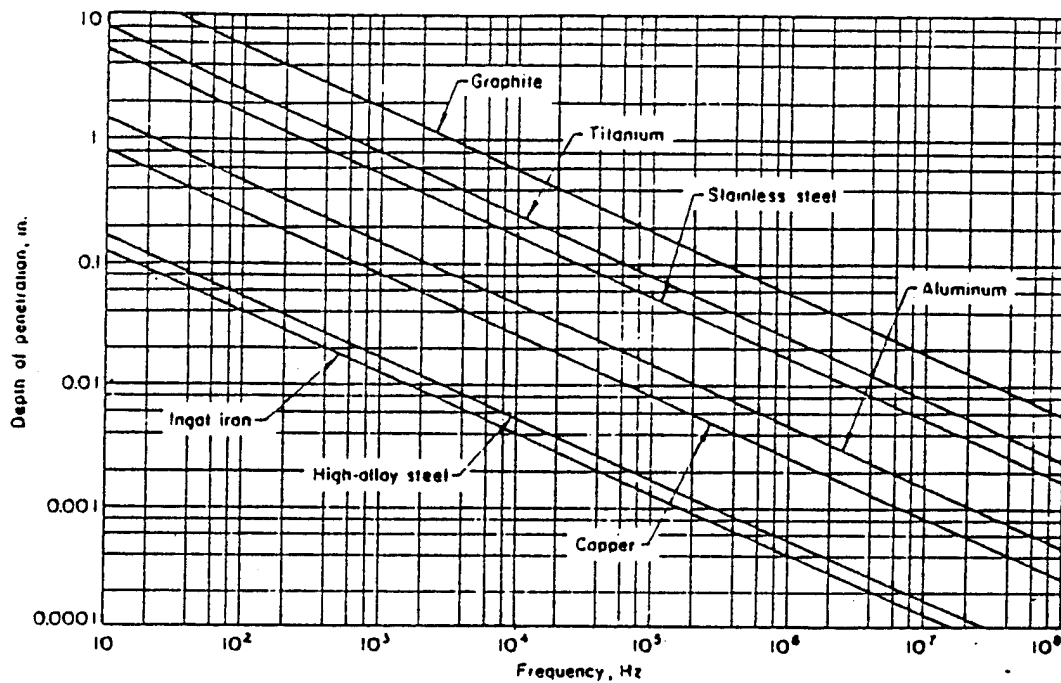
16

Figure 2.6 Standard depths of penetration as a function of frequency used in eddy current inspection for several metals of various electrical conductivities. From Ref. [8].

D. PRECIPITATION HEAT TREATMENTS

1. Background

The purpose of precipitation heat treatment is to enhance the strength and hardness of appropriate metallic alloys. This is accomplished by heat treating such an alloy in a manner that produces extremely small, uniformly dispersed particles of a second phase within the original matrix. These finely dispersed particles act as barriers to dislocation movement and thereby increase strength.

The history of heat treatment can be traced back beyond when man first heat treated a sword made from an iron-carbon alloy. It was discovered that if the sword were heated until it glowed red and then plunged into water, it would become very hard but too brittle for use. If the sword were then reheated to a lower temperature it could be made useable again [Ref.15]. Over time, the art of hardening heat treatment has transformed

17

into a science. Using theoretical models, statistical process control is now being employed. These models attempt to account for all possible influences in an attempt to produce a perfect product every time. The sheer number of variables, however, prevents the achievement of exact values for material properties consistently. The need for "real time" evaluation of the process is the next step in developing this discipline.

Precipitation hardening is basically a three step process: (1), solution heat treatment; (2), quenching, and (3), subsequent precipitation heat treatment. All of these play important roles in the properties developed in the final product. Figure 2.7 graphically illustrates the three steps of the process used to achieve a -T6 temper in an Al 7075 sample. To further explain the process, a phase diagram for the particular alloy is required. The Al 7075 alloy used in this thesis is a quaternary system, i.e. a system with three main alloying elements, with a rather complicated phase diagram. In order to simplify the discussion, a hypothetical binary system phase diagram will be employed [Fig. 2.8]. There are four requisite features in order for a material to be capable of precipitation hardening [Ref. 7]. First, there must be an appreciable maximum solubility of one component in the base metal. Secondly, the solubility limit must rapidly decrease in concentration of the major component when there is a decrease in temperature. Next, the composition of the alloy must be less than the maximum solubility. Finally, lattice strains must be established at the precipitate-matrix interface. This last requirement is achieved by a lattice mismatch creating a strain field around the growing precipitate. Figure 2.8 clearly shows the first three conditions for an alloy of composition C_o. The maximum solubility, point M, is to the right and larger than the alloy composition, while the low temperature solubility, point N, is smaller.

The heat treatment process for this hypothetical alloy consists of solution heat treating the material at T_o, for a predetermined time, to produce a homogeneous solid solution. The alloy is then quenched to T_1, at a predetermined cooling rate, in order to trap the solute atoms and excess vacancies in solution. This develops a metastable, supersaturated, condition. Finally, the alloy is reheated to T_2, for a suitable time, which
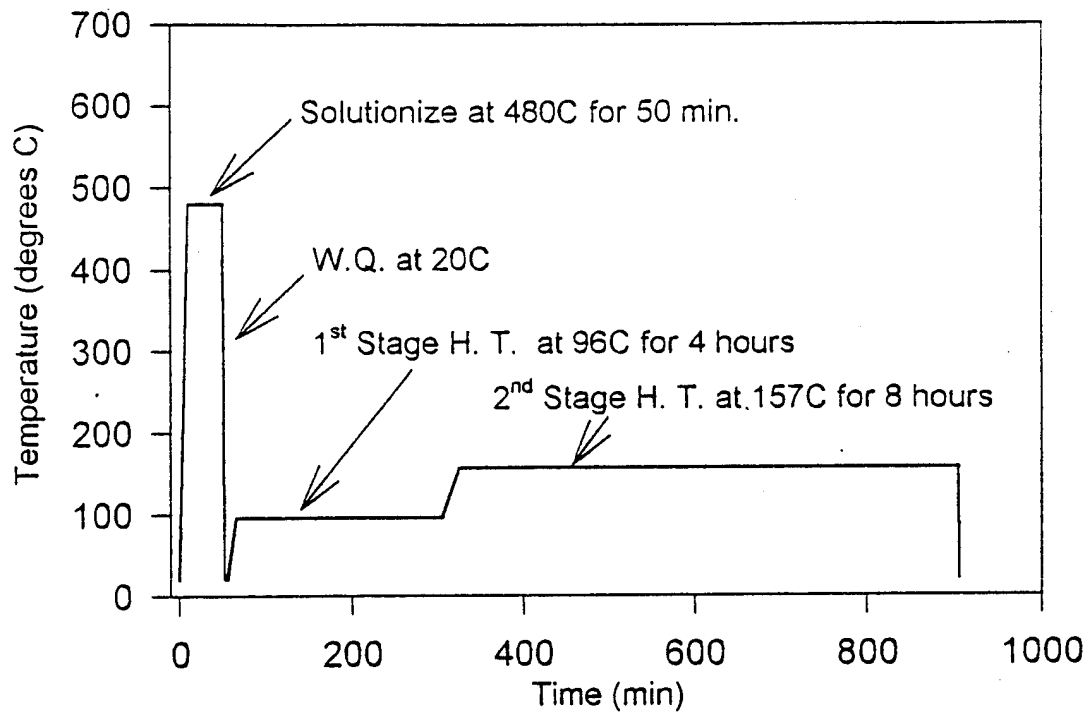
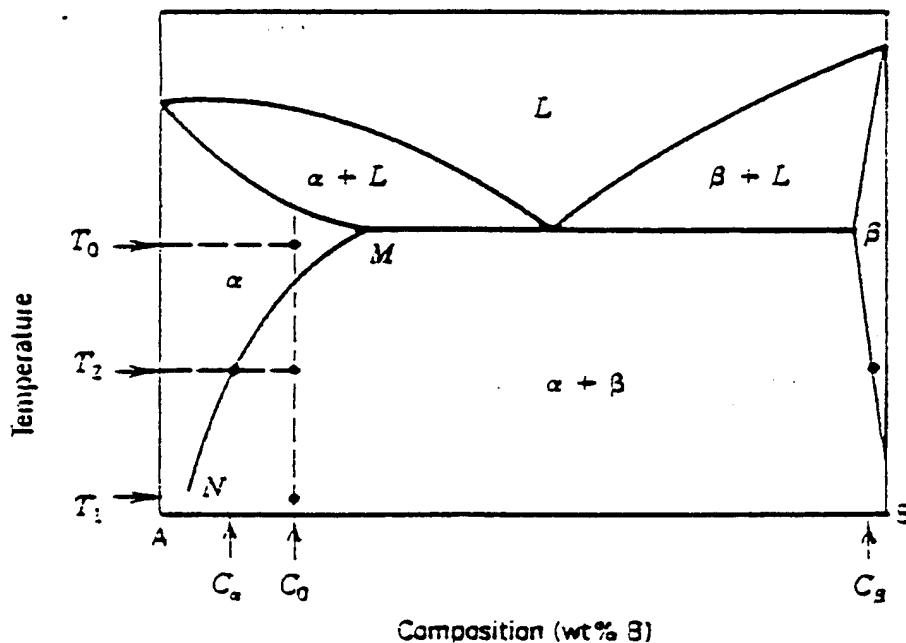**Figure 2.7   Typical two-stage heat treatment to achieve a -T6 temper in an Al 7075 alloy.**

Figure 2.8   Hypothetical phase diagram for a precipitation hardenable alloy of composition C_o. From Ref. [7].

allows for solutes to diffuse through the matrix to form precipitates. These precipitates continue to grow with time following a sequence of phases characteristic of the alloy. These changes in microstructure during the heat treatment process create corresponding changes in material properties. The detailed microstructural changes that occur depend on the particular alloy, its fabrication history and the temperature and duration of the heat treatment [Ref. 16].

2. Phase Changes During Precipitation in Age-Hardenable Alloys

As discussed in the previous section, the purpose of the solution heat treatment is to produce a homogeneous solid solution. This is accomplished by heating the alloy to a temperature high enough so that second phases initially present will dissolve into the matrix. Upon quenching, these dissolved solute atoms, and the excess vacancy concentration associated with higher temperatures, are trapped in the matrix. This forms a metastable, supersaturated, solid solution. When exposed to subsequent heat treatments, these trapped solutes and vacancies diffuse, driven by a reduction in the free energy of the material. The form, or intermediate phases, these precipitates adopt is dependent on the composition of the alloy and the temperature of the treatment. Figure 2.9 shows the phases possible in the Al-Cu alloy system. When a supersaturated solid solution is aged at a temperature just below the G.P. solvus line, the rate of formation of G.P. zones is greater than the other possible decomposition products because their formation provides the maximum rate of decrease of free energy. The θ" phase has the next highest rate of formation and nuclei of this phase will form on prolonged aging. The precipitation process will continue with time at temperature, until the most stable phase, θ (Al_2Cu), is produced [Ref. 10].

The strength of the alloy is directly related to the prevailing phase. Figure 2.10 shows that the strength initially increases reaching a peak strength and then, with time, gradually decreases. This can be explained with a discussion on particle size and coherency with the matrix. The G.P. zones are created by homogeneous nucleation
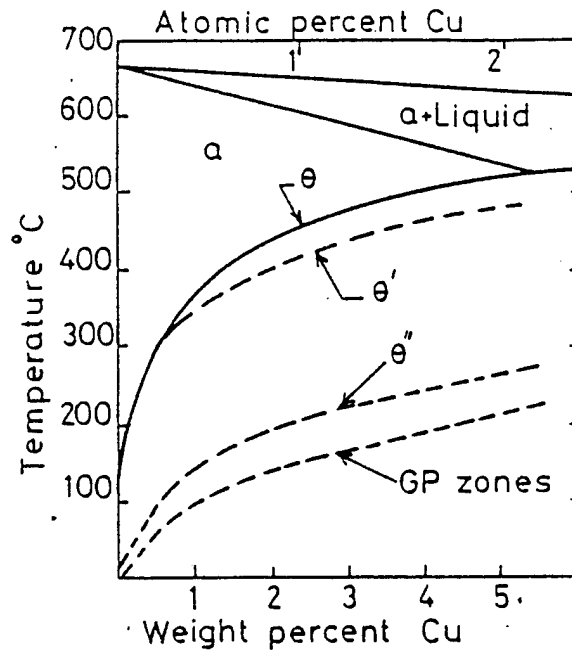
Figure 2.9 Al-rich Al-Cu binary diagram showing GP, θ", θ', and solvus lines. (Reproduced from G. Lorimer, Precipitation Processes in Solids, K. C. Russel and H.I. Aaronson (Eds.), The Metallurgical Society of AMIE, 1978, p. 87 , D.A. Porter and K. E. Easterling, Phase Transformations in Metals and Alloys, Van Nostrand, Rheinhold (UK), 1987, p. 291, and Ref. [2].
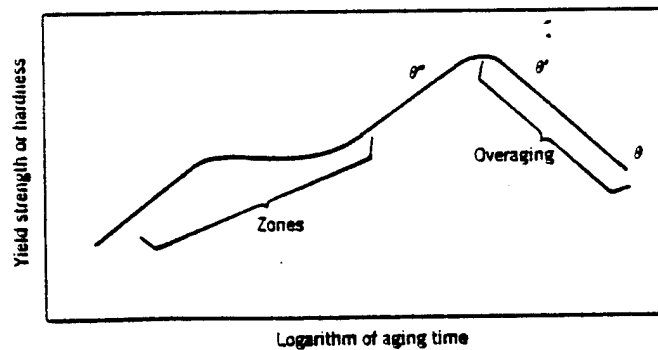

Figure 2.10 Schematic showing tensile strength and hardness as a function of the logarithm of aging time at a constant temperature during the precipitation heat treatment. From Ref. [7].

21

within the matrix which is accelerated by the increased vacancy concentration retained during the quench. These zones are local segregation of solute atoms which maintain complete coherency with the matrix. Due to this segregation and coherency, there is a mismatch in size between such clusters and the matrix creating a lattice strain. Because of the considerable size difference in Al-Cu alloys, these zones form as very small disks. As these zones grow and transform into the θ" phase, coherency is maintained and the strain field increases. Figure 2.11 (a&b) shows the developing strain field as the precipitates grow. This strain creates interference in the motion of dislocations which results in an increased strength. As growth continues, and the θ' phase evolves, the interface becomes semi-coherent, which reduces the strains, and thus, reduces the strength. This loss of strength is known as overaging. Finally, when the equilibrium θ phase is reached, the interface is completely incoherent [Fig. 2.11 (c)] and spacing of precipitate particles becomes so large that dislocations are able to bow readily between the precipitates [Ref. 7].
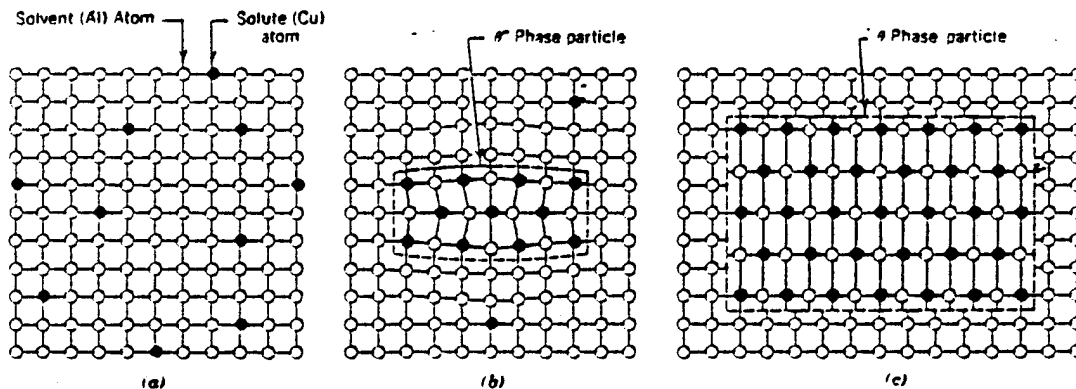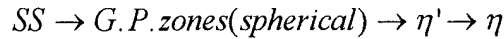

Figure 2.11 Schematic depiction of several stages in the formation of the equilibrium precipitate (θ) phase. (a) A supersaturated solid phase. (b) A transition, θ", precipitate phase. (c) The equilibrium θ phase. From Ref. [7].

In the Aluminum-Zinc-Magnesium (Al-Zn-Mg) alloys, the size difference is less than in the case of the Al-Cu alloys and the zones produced are spherically shaped. Again, with increased time, these zones continue to grow, change form, and the strength will follow a similar curve as shown for the Al-Cu alloy. The typical aging sequence followed by an Al-Zn-Mg alloys is:

$$SS \rightarrow G.P.zones(spherical) \rightarrow \eta' \rightarrow \eta$$

where η is the equilibrium phase, $MgZn_2$. Depending on the composition, the sequence and equilibrium phase may vary as do the material properties obtained.

Like most mechanical properties, the resistivity of an alloy is also dependent on the microstructure. As discussed earlier in this Chapter, the strain fields created around the G.P. zones decrease the mean free path of the conduction electrons, thus initially increasing the resistivity. As the zones transform through the transition phase, η', to the equilibrium phase, η, the resistivity begins to slowly decline as more and more solutes are taken out of solution. This decrease in solute atom concentration, within the matrix, lowers the number of scattering events enough to offset the effect of the strain field. With increased temperature comes an increase in diffusion and a higher rate of precipitate growth is obtained. This increased rate of growth corresponds to a more rapid decrease in resistivity.

3. Heat Treatment Process

The ASM Handbook [Ref. 15] recommends two methods in the heat treating of Al 7075 in order to achieve the -T6, high strength, temper. The first is a single-step process of reheating the solutionized material to 120° C for 24 hours. Figure 2.12 shows that using temperatures higher than 120° C (250° F) would result in a loss of peak strength. The alternative to this lengthy single-step process is a multi-step heat treatment of 4 hours at 96° C followed by 8 hours at 157° C [Fig. 2.7]. As can be seen, the time has been cut in

half yet the peak strength will still be achieved. This occurs despite the fact that
isothermal aging above 120° usually provides a much lower strength. The reason is that
the initial low-temperature treatment develops a fine distribution of G.P. zones which
grow to a sufficient size to be stable when the temperature is increased. Using a single,
higher temperature would result in coarser and more widely distributed particles [Ref. 10].
There are many reasons why a commercial heat treater would select one method over the
other. Time, cost, and the probability of obtaining the intended properties are all
considerations. By increasing the temperature, the probability of obtaining exactly what is
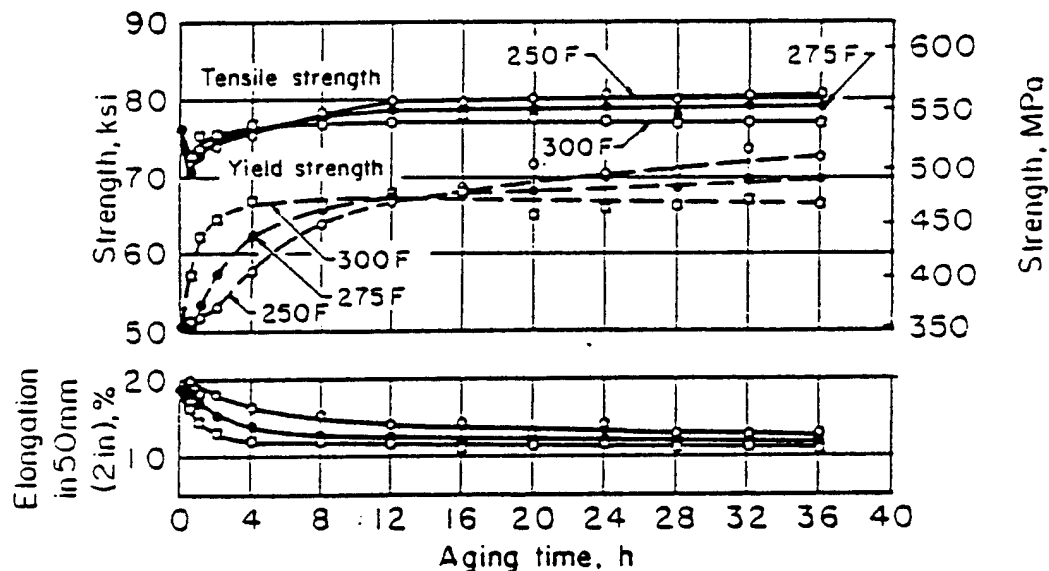desired is reduced [Ref. 16].

**Figure 2.12   Aging of Al 7075 sheet at 120° to 150°C (250 to 300°F). From J.A.
Nock, Jr., Alcoa Research Laboratories, and Ref. [16].**

To achieve the -T73 (stable) temper in an Al 7075 sheet, a two-stage treatment of
6 to 8 hours at 107°, followed by 24 to 30 hours at 163° C, is recommended. Again,
experience plays a major role in determining the necessary times. Figure 2.13 shows that
variations in the second step soak time of several hours and soak temperature of up to 11°
is enough to produce a 150 MPa variation in strength. Similar variations around the

recommended single-step heat treatment to produce the -T6 temper affects strength by only 28 MPa. Thus, control of temperature and time to achieve required mechanical properties for the -T73 temper is more critical [Ref. 8]. The reason for this wide variation is that the higher second-step temperature facilitates a significantly faster rate of microstructural change. Another factor to consider is the rate of heating from the first to the second stage temperature. During this period precipitation occurs which must be taken into account.
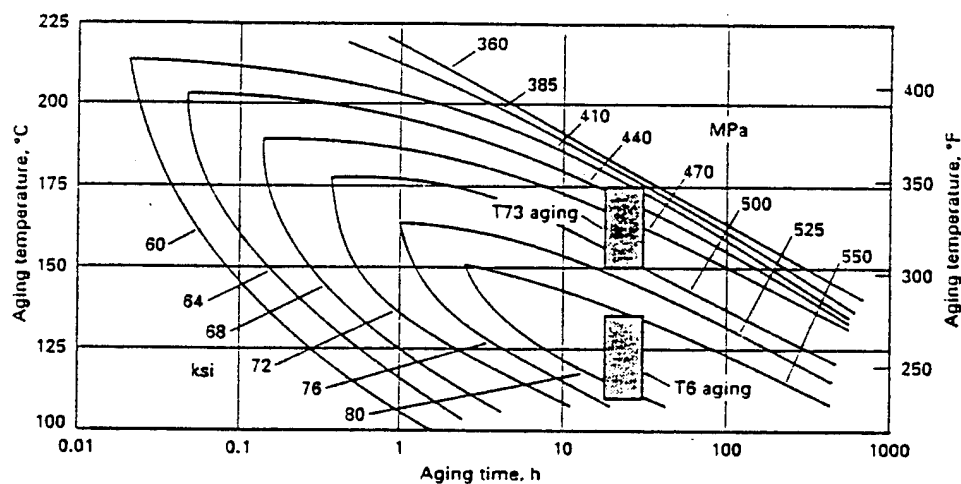

Figure 2.13 Iso-yield strength curves for alloy Al 7075. From Ref. [8].

III. EXPERIMENTAL PROCEDURES AND COMPONENT DESIGN

A. INITIAL SENSOR SYSTEM AND MODIFICATIONS

The original design of the sensor system by Esarey [Ref. 1] consisted of a base plate on which the samples were placed, various support bars and two probe coils which were lowered onto the samples with a "lifting cam". This design lacked the ability to achieve consistent positioning of the sample and probe coils. Another drawback to Esarey's [Ref. 1] initial system was that the bridge output was in RMS voltage and achieving an initial null (or balanced) condition at the start of an experiment was extremely difficult. Mata's [Ref. 2] follow-on design consisted of an apparatus with inverted coils so that the samples could be placed on top of the coils, and alignment notches were cut in the supports to provide a more uniform placement. He also incorporated the impedance bridge circuit into a Bridge Carrier Amplifier/Filter (BCA) which synchronously demodulated the bridge output signal. This provided for an easily attainable null and an amplified output signal. The apparatus, as modified by Mata [Ref. 2], is shown schematically in Fig. 3.1. This equipment proved adequate for the purpose of performing the present work with only one modification. The system, as designed, lacked the ability to directly monitor the temperature of the samples as they went through the heat treatment process. In Mata's [Ref. 2] work, the test temperature was assumed to be the oven temperature. To resolve this deficiency, two K-type thermocouples were connected to the apparatus with a lever and spring device. The two wire ends of the thermocouples were separated so that an intermediate metal connection would be made upon contact with the sample, which then provided the sample temperature. The lever and spring system was designed to minimize interference with rapid placement of samples in the test apparatus. This modification to the system can be seen in Fig. 3.2.
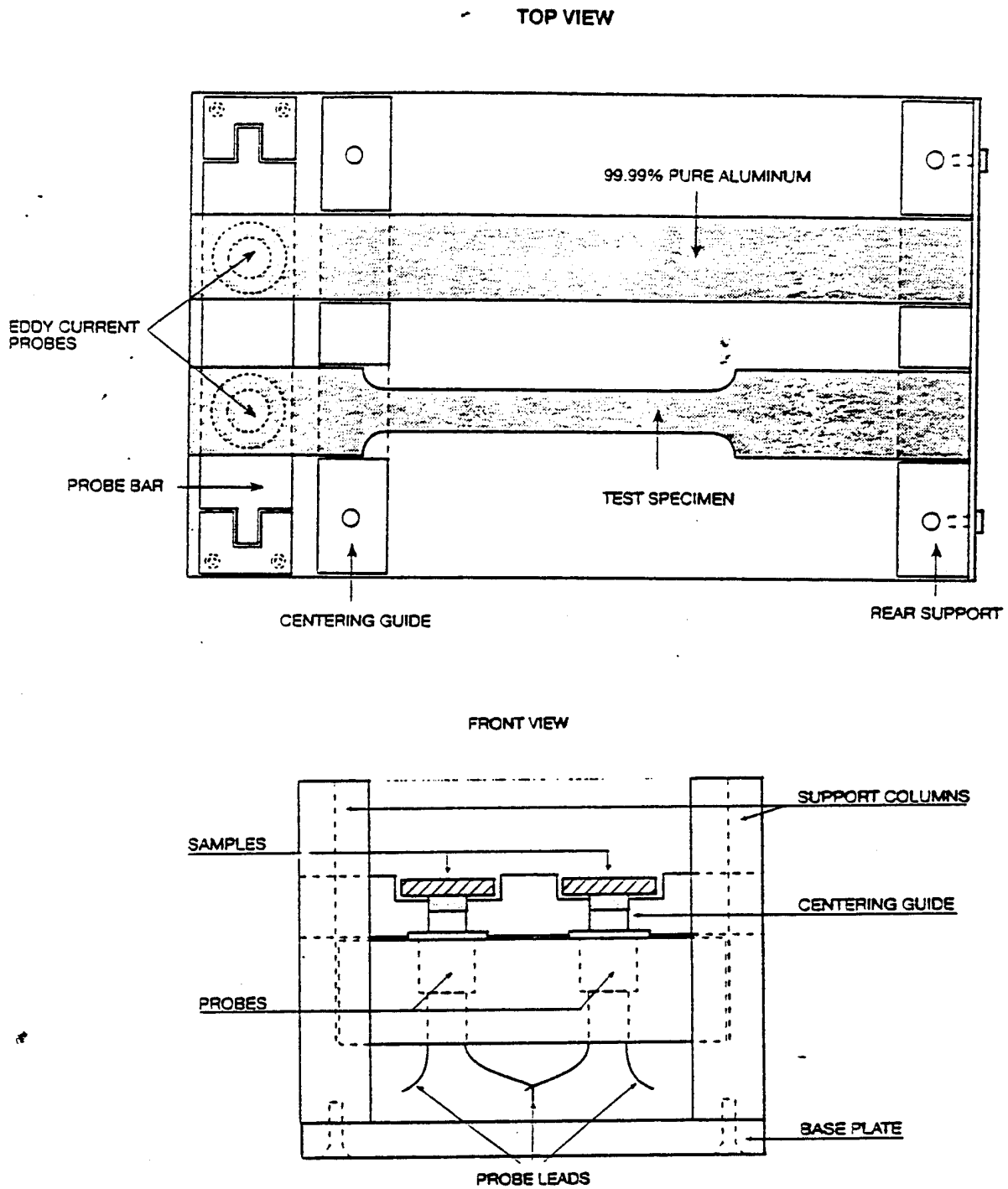
TOP VIEW

99.99% PURE ALUMINUM

EDDY CURRENT
PROBES

PROBE BAR

TEST SPECIMEN

CENTERING GUIDE

REAR SUPPORT

FRONT VIEW

SUPPORT COLUMNS

SAMPLES

CENTERING GUIDE

PROBES

BASE PLATE

PROBE LEADS

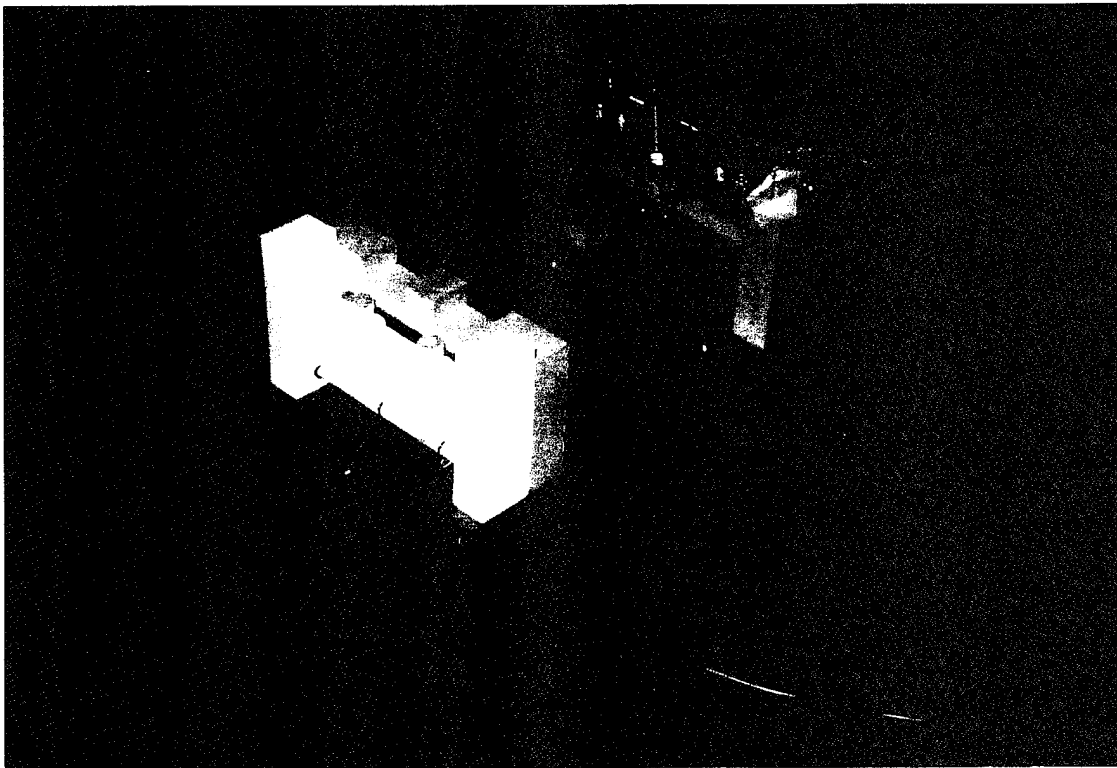Figure 3.1 Schematic drawings of testing apparatus. From Ref. [2].

Figure 3.2   Photograph of testing apparatus, test probes and thermocouple device.

B. EXPERIMENTAL PROCEDURE

As described in Chapter II, there are basically three steps in the heat treatment process: solution heat treatment; quenching; and a precipitation heat treatment. The testing procedures performed incorporated these three steps with additional steps to obtain the aging progress data. For each experiment, the bridge was initially nulled, using two identical pure aluminum samples at the desired first stage testing temperature, by adjusting the BCA. The step-by-step procedures followed are outlined below:

(1) The convection oven was set at the desired first stage aging temperature with the apparatus inside and two identical, pure aluminum samples on each probe coil. Set point temperatures were accurate to within +/- 2° C.

(2) With isothermal furnace conditions verified and all system component settings and circuit connections verified, the data acquisition program was given the desired instructions regarding timing of sampling intervals for measuring the bridge unbalance voltage.

(3) After allowing the system to settle at the first stage temperature, the bridge output voltage was nulled by adjusting the BCA.

(4) The Al 7075 test samples were solutionized at 480° C (+/- 2° C) for 50 minutes.

(5) Samples were quickly quenched in a large water tank at approximately 20° C.

(6) The sample was removed from the quench and thoroughly dried in preparation for inserting into the furnace.

(7) Upon opening the furnace, the thermocouples were lifted, one of the pure aluminum samples were removed, and the test sample was inserted in its place. The thermocouples were then lowered onto the samples and the furnace was closed as quickly as possible.

(8) The data acquisition program was then started, generating time versus BCA output voltage data files based on instructions given in step 2.

(9) The test sample was removed and quenched at the conclusion of the heat treatment process and kept in cold storage to await mechanical testing.

C. MAJOR MONITORING SYSTEM COMPONENTS

The following is a brief description of the major monitoring system components and their function in the operation of the eddy current sensing system.

1. Testing Apparatus

The testing apparatus, as modified by Mata [Ref. 2] and shown in Fig. 3.1, consisted of a base plate, a rear sample support, a centering guide for consistent placement, a probe bar support and the probe bar which held the inverted probe coils in position. This design proved adequate for the testing of completely flat samples but cannot compensate for the distortion of samples during the quench procedure. As will be discussed in the following chapter, this shortcoming leads to a lift-off effect in the BCA voltage versus time data obtained. The only problem that this effect seems to generate, however, is a consistent variation of the initial unbalance voltage. The BCA voltage output versus time curves produced still follow the same path for identical heat treatments.

2. Probe Coils

The two probes designed by Esarey [Ref. 1] provided a means to induce the eddy currents into the samples and acted as two opposing elements in an impedance bridge circuit in order to monitor the change (or unbalance) in resistivity between a reference sample and the test sample. This type of design, known as an absolute coil arrangement [Ref. 8], allows for comparison of an unknown sample to a known standard. The probes were designed with a minimum footprint to decrease thermal shielding of the test sample and minimize any local retardation of the aging process [Ref. 1]. This reduced footprint also eliminated the possibility of edge effects.

3. Bridge Carrier Amplifier/Filter (BCA)

The BCA, designed by Christian [Ref. 17], measures the changes in inductive reactance between two probe coils connected in a bridge configuration (Fig. 3.3) and thus provides a means of detecting changes in resistivity. The BCA system components include

an oscillator set at 5 volts RMS and 52 KHz (based on test probe type and size), a 500 gain instrumentation amplifier, a phase-sensitive demodulator, an amplifier/filter to refine the output signal, and an RMS converter. A schematic of the BCA is shown in Fig. 3.4. This device provides an amplified input signal to the bridge circuit and then synchronously demodulates the bridge output so that the signal can be balanced, or nulled. It then filters the signal and amplifies it to an output range of +/-10 volts direct current (dc).

An equation for the BCA output voltage (V_o) was given by Esarey [Ref. 1] and Mata [Ref. 2] as follows:

$$V_o = \left(\frac{Z_1}{R_L + Z_1} - \frac{Z_2}{R_R + Z_2} \right) * V_i \tag{3.1}$$

where Z_1 is the magnitude of the reference probe impedance, R_L is the resistance of the upper left bridge leg, Z_2 is the magnitude of the testing probe impedance, R_R is the resistance of the upper right bridge leg , and V_i is the input voltage [Ref. 2].

4. Digital Multimeter

The digital multimeter was used to obtain accurate and continuous measuring of the BCA voltage output. It also provided a computer interface for input of measured voltage values into the data acquisition file.

5. Data Acquisition Personal Computer (DAPC)

The DAPC was used to receive and store BCA voltage output data from the digital multimeter and elapsed time data at intervals specified in the data acquisition program. It was then used to generate the voltage versus time plots used for analysis of the aging process.
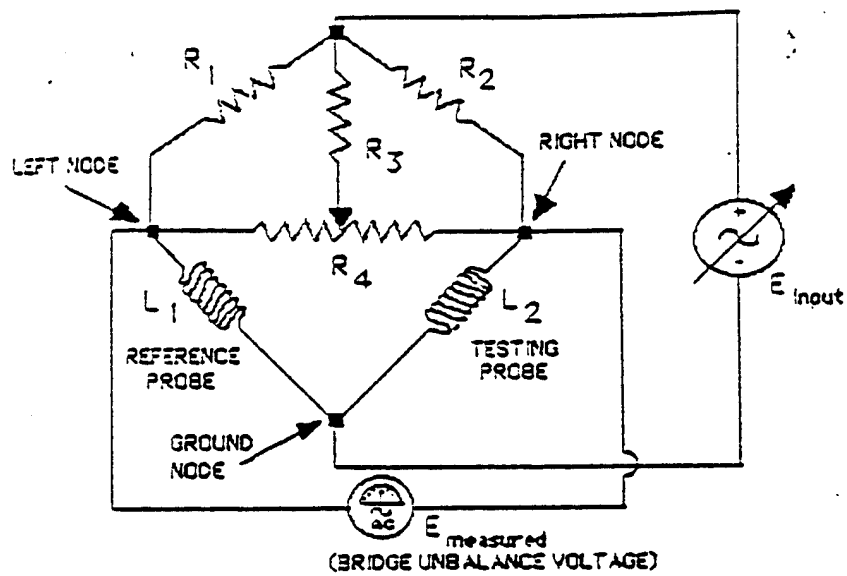
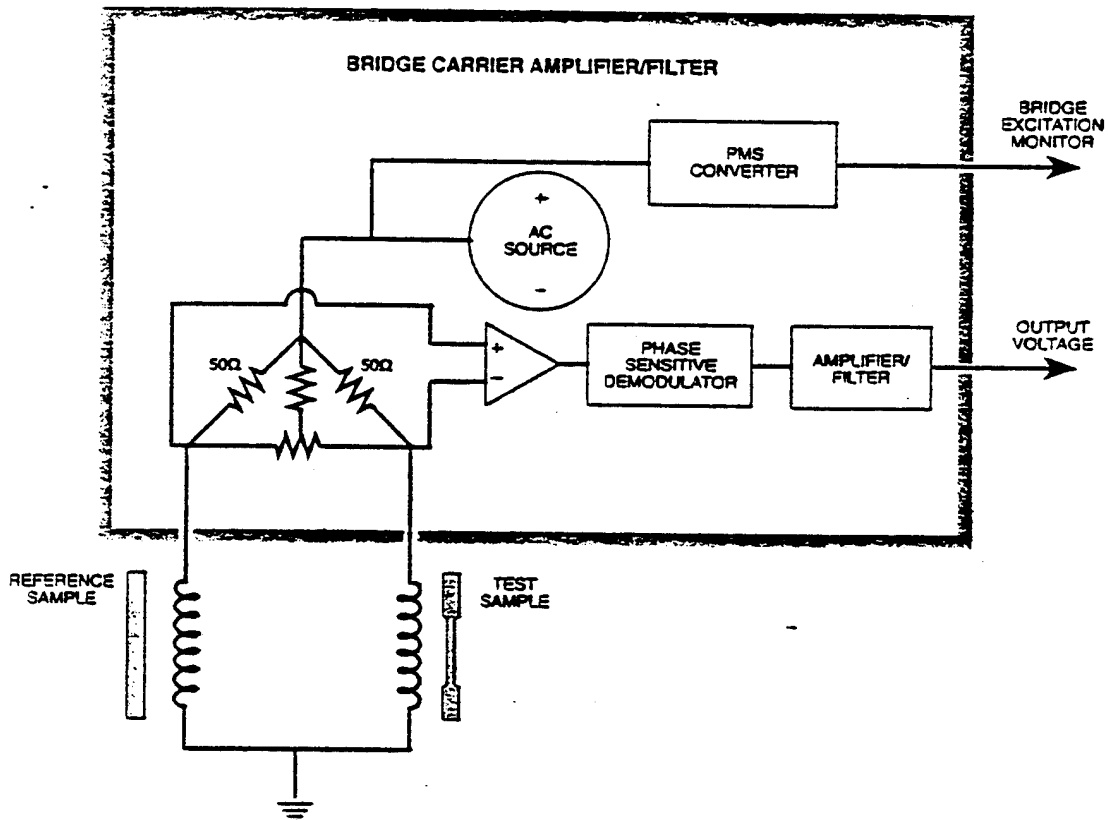Figure 3.3   Simplified impedance bridge circuit drawing.   From Ref. [2].

Figure 3.4   Block diagram of Bridge Carrier Amplifier/Filter.   From Ref. [2].

IV. RESULTS AND DISCUSSION

The eddy current monitoring system devised by Esarey [Ref. 1] was designed with the goal of providing a more precise monitoring and control of the heat treatment process. However, before feedback control capability can be established it is necessary to more clearly understand the capabilities and limitations of the system itself. The primary focus of this thesis was twofold: (1), to assess the sources of variability in the BCA voltage versus time plots; and (2), interpret the BCA voltage output curves generated by the eddy current monitoring system.

A. MONITORING SYSTEM DESIGN AND OPERATION

The monitoring system, as described in Chapter III, proved to be very easy to operate and experienced no mechanical problems through more than 100 testing cycles. However, the apparatus lacked the ability to monitor test specimen temperature throughout the heat treatment process. In earlier work [Ref. 1 & 2], oven temperature only was recorded. This ability is critical because of the importance of temperature in the aging process. Sample temperature was also important in this research in order to answer questions involving the BCA voltage output during temperature transients, as will be discussed later in this chapter. Attaching K-type thermocouples as described in Chapter III, to both the reference and test samples gave the apparatus this required ability. An example of the temperature versus time plots generated is shown in Fig. 4.1(a). As can be seen, when the oven door is opened to insert the test sample, the pure aluminum reference sample experiences a slight decrease in temperature while the test sample immediately starts to heat up. After approximately four minutes, the two samples are very nearly in thermal equilibrium at the first-stage heat treatment temperature. Figure 4.1(b) is the BCA voltage versus time plot for this particular experiment. It shows that during this first transient, the BCA voltage rapidly increases. The reasons for this will be discussed later in this Chapter. Throughout the first stage, the temperature of the two samples remains
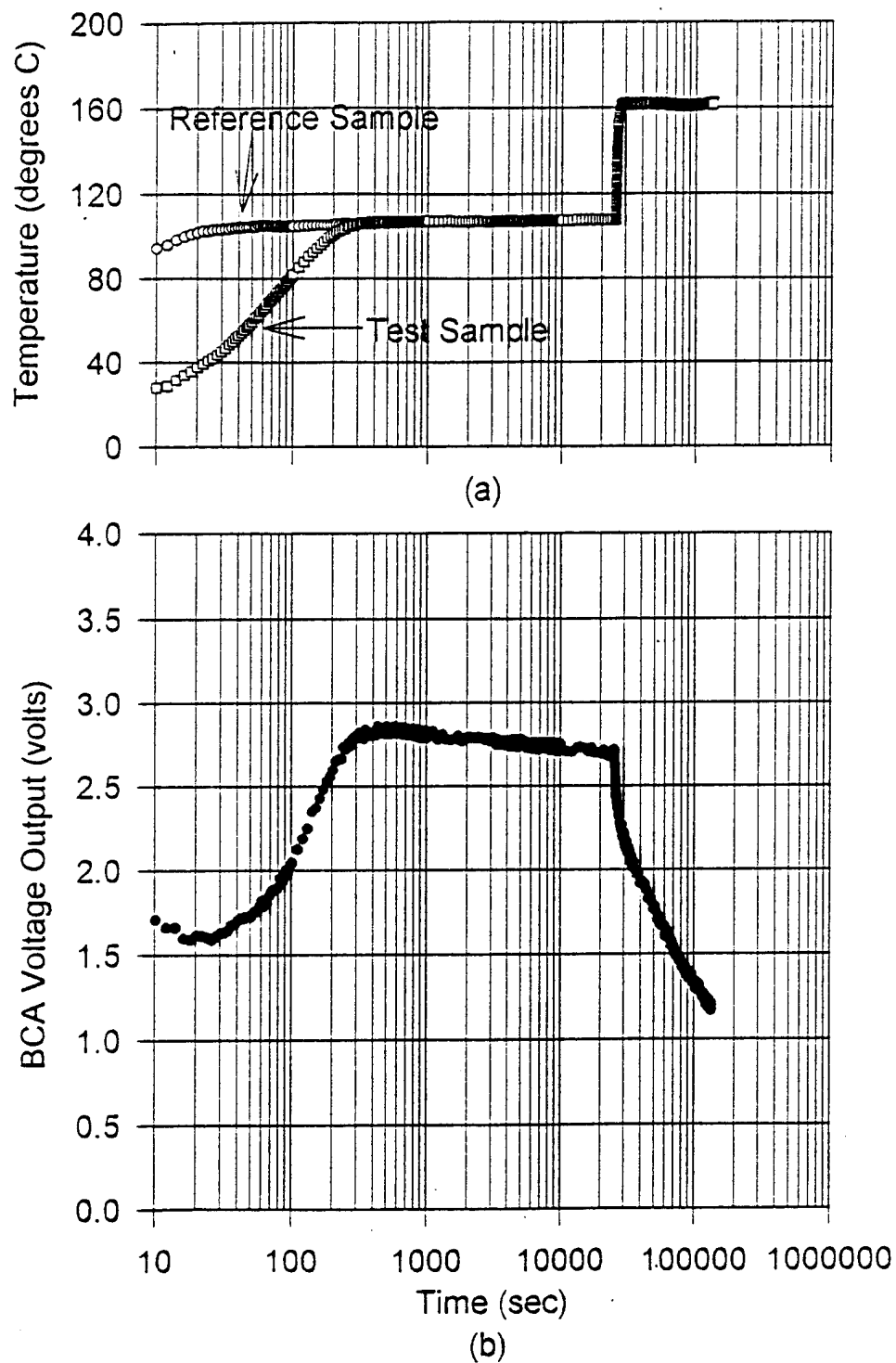
Figure 4.1   System output for a two-stage heat treatment. (a) Typical sample
temperature versus time plot. (b) Typical BCA voltage output versus time curve.

unchanged while the BCA voltage experiences a gradual decline due to the aging process.

During the step increase in temperature for the second-stage of the heat treatment process, the temperature of the two samples increase at nearly the same rate, with the alloy test sample lagging behind by as much as 10 degrees due to a lower thermal conductivity. The rapid decline of the BCA voltage during this transient will be discussed later in the Chapter. Finally, at the conclusion of this transient region, the two samples are in thermal equilibrium with the oven temperature. The BCA voltage again undergoes a steady decline in value but this time at a greater rate due to the acceleration of precipitate growth at the higher temperature.

A remaining weakness of the current system is the inability to accommodate distortion, or warpage, of the test sample that occurs during quenching after solution treatment. Such distortion causes lift-off differences from sample to sample and subsequent variation in the initial voltage output. This results, in turn, in a constant output voltage shift in subsequent aging curves. This is clearly shown in Fig. 4.2(a&b). Figure 4.2(a) shows the BCA voltage curves of five Al 7075 samples which had all undergone the same heat treatment process. The only difference was the times held at the second stage temperature. As can be seen, the initial BCA voltage output varied from 1.7 to 3.2 volts. Note that when the curves are normalized to a selected peak voltage, Fig. 4.2(b), they lie on top of one another. A different design to accommodate for this change in sample geometry is recommended, and is currently being developed.

B. SYSTEM CALIBRATION

As part of system calibration, two pure aluminum samples (99.99%) were fabricated from the same ingot. These identical samples were placed in the apparatus and the voltage output signal was nulled at ambient temperature. In theory, with increasing temperature of the furnace which contained the apparatus, the voltage output should have remained at the null setting. This was not the case. Instead, a non-linear increase in voltage with increasing temperature was observed. The temperature of the two pure
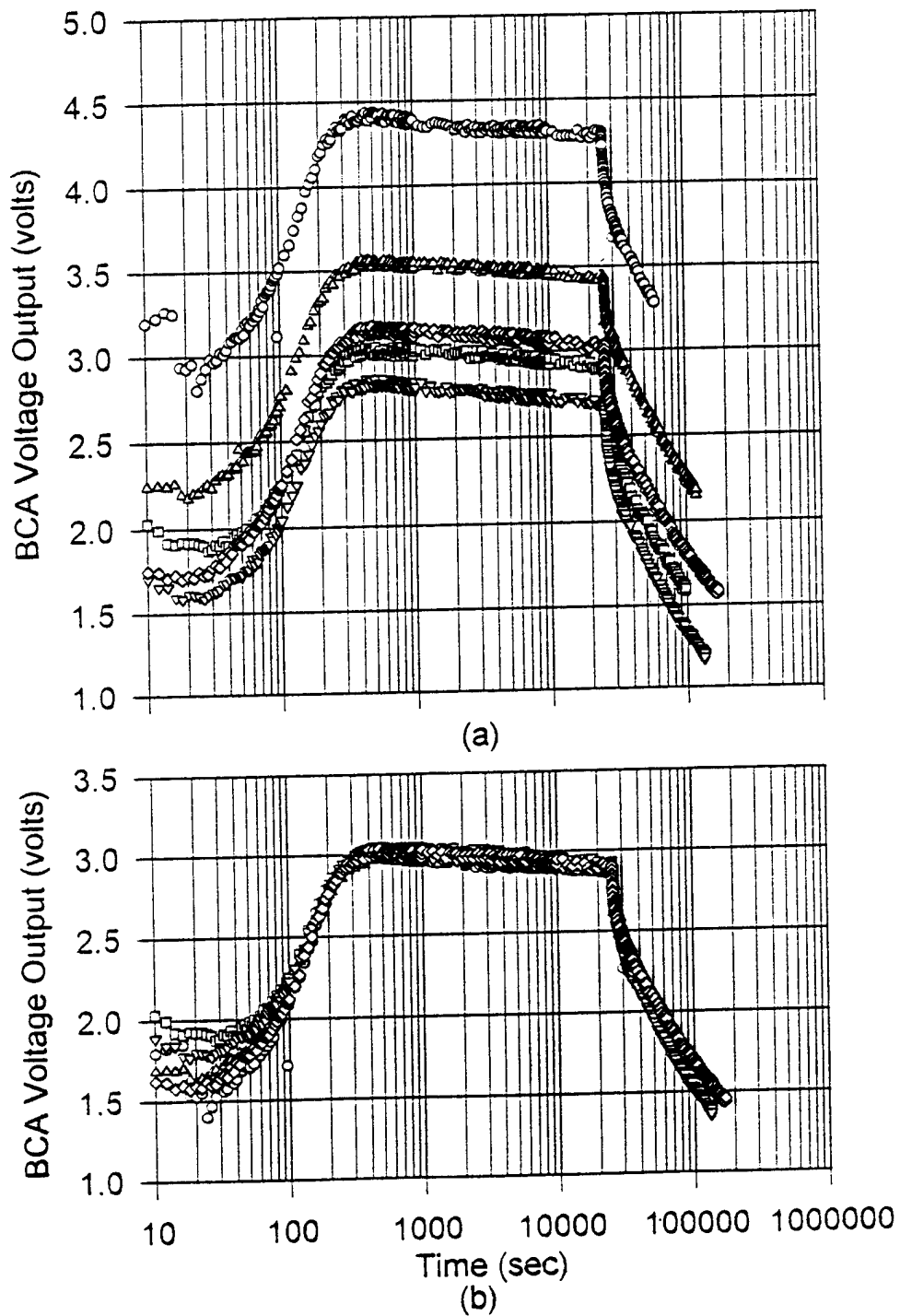
Figure 4.2 System output for five similar two-stage heat treatments. (a) Shows variability in initial BCA output. (b) Shows similarity in curves when normalized.

aluminum samples was incrementally increased and allowed to stabilize. At each temperature, as shown in Fig. 4.3, a stable value of this offset voltage was obtained. This indicates that the offset is only temperature dependent. After attaining the highest temperature, the furnace was shut off and the samples and apparatus were furnace cooled. A plot of the voltage offset versus temperature was then generated during this cool down period (Fig. 4.4). These data represent the voltage offset relative to ambient for a given test temperature and would have to be accounted for in heat treatments involving a change in temperature. This voltage offset may be accounted for when the system is nulled at test temperature for isothermal use of the system.

Mata [Ref. 2] surmised that the offset was a function of material differences between the pure aluminum samples he was using in his initial nulling step. Because the pure aluminum samples were from the same stock, it is now believed that the offset is a function of the mismatch between the two eddy-current coils. The coils used in the monitoring apparatus had been hand wound. This method of fabrication makes it nearly impossible to create two identical probes. Variables such as number of turns of wire, spacing between turns, and inconsistent tension could individually or additively account for the voltage difference observed. As temperature increases, uneven thermal expansion of the wired coils would create a different path for current through each probe. In future designs, it is recommended that professionally wound coils be acquired to minimize this problem.

C. G.P. ZONE FORMATION

The monitoring concept was determined to be valid as verified by a series of experiments involving room temperature G.P. zone formation. An age hardenable material begins to show an increase in strength corresponding to the formation of G.P. zones. These zones create a stress field which act as barriers to dislocation movements. As these zones grow, the stress field becomes more extensive and the strength of the material increases. During room temperature aging of a solutionized Al 7075 sample,
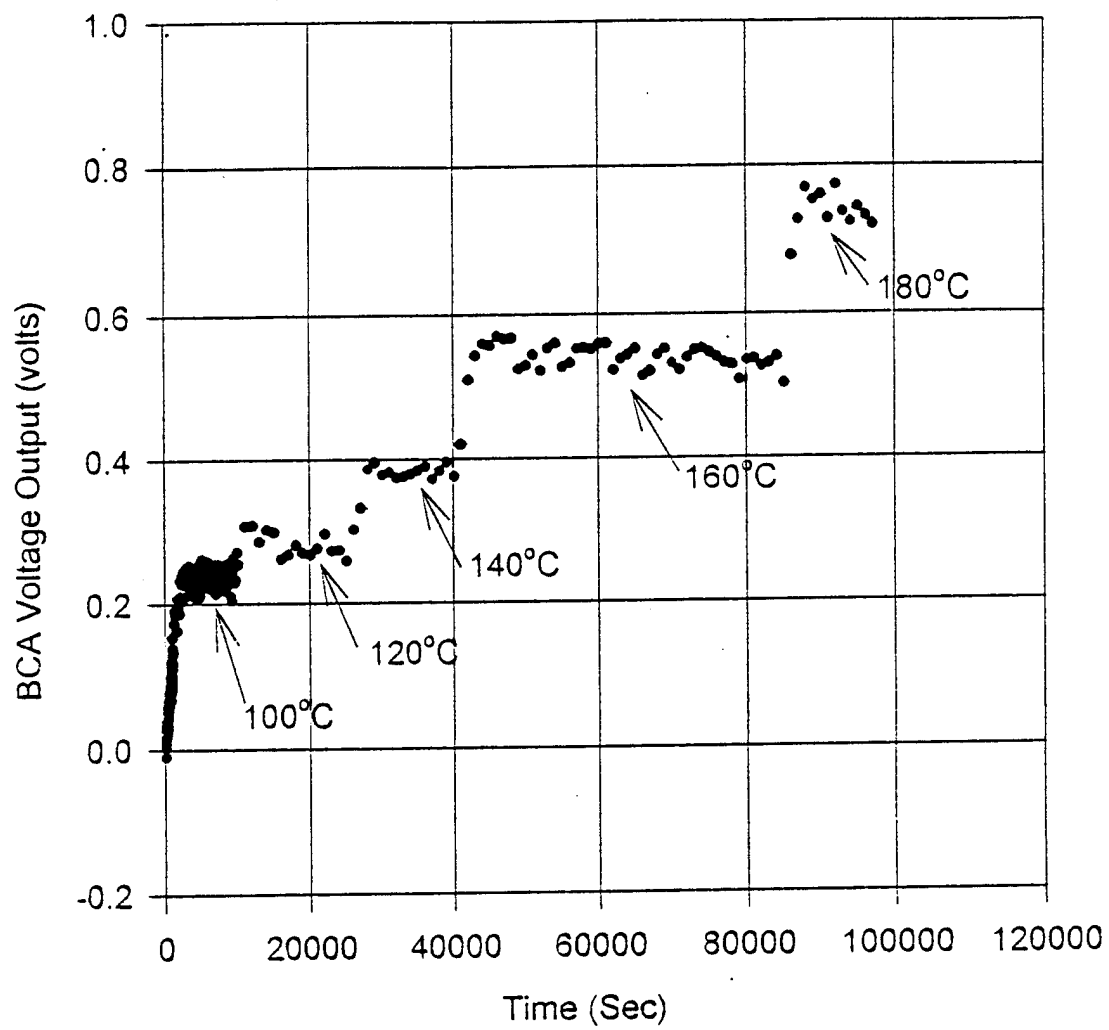
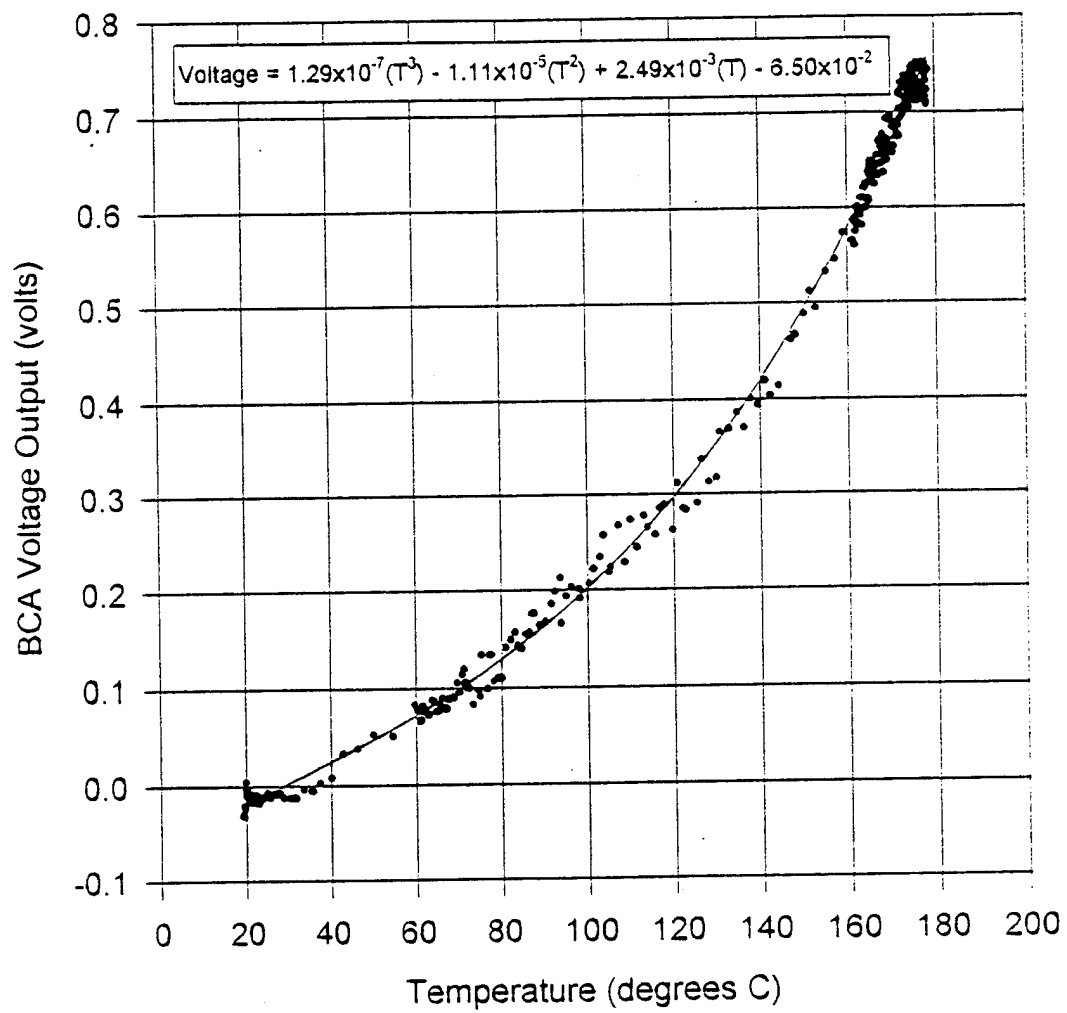**Figure 4.3   Apparent BCA voltage offset with temperature.**

Figure 4.4   Voltage offset relative to ambient temperature.

The figure shows a plot of BCA Voltage Output (volts) on the y-axis versus Temperature (degrees C) on the x-axis, with the fit equation:

$$\text{Voltage} = 1.29 \times 10^{-7}(T^3) - 1.11 \times 10^{-5}(T^2) + 2.49 \times 10^{-3}(T) - 6.50 \times 10^{-2}$$

increases in yield and tensile strengths begin after approximately 45 minutes of aging as shown in Fig. 4.5. In room temperature aging of a solutionized and water quenched Al 7075 sample, the eddy current sensor system indicated a distinct rise in BCA voltage output beginning at approximately 50 minutes (3000 seconds) of aging (Fig. 4.6). This increase is indicative of the increased electrical resistance of the material as a result of the G.P. zone formation. Using an elevated test temperature (40° C), the onset of aging was accelerated (as determined by BCA output) due to the acceleration of the diffusion-controlled nucleation and growth process (Fig. 4.6). When a solutionized sample is quenched relatively slowly, a number of the vacancies, which contribute to the diffusion process of G.P. zone formation, are able to diffuse out. A test conducted using an oil quench after solution heat treatment revealed a delay in the onset of G.P. zone formation, again as reflected in a delay in increased BCA output (Fig. 4.6). Figure 4.7 shows results for two identical samples initially solutionized, water quenched, and then inserted into the apparatus set at 107° C. These were allowed to reach thermal equilibrium with the reference sample (at about 600 seconds). Then, the samples were removed, quenched to room temperature, and reinserted into the apparatus. The difference between the two curves clearly show the role that G.P. zone formation plays in the BCA voltage output.
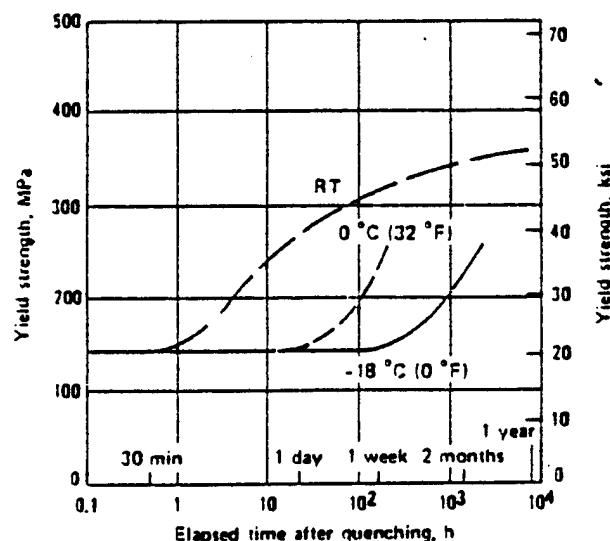

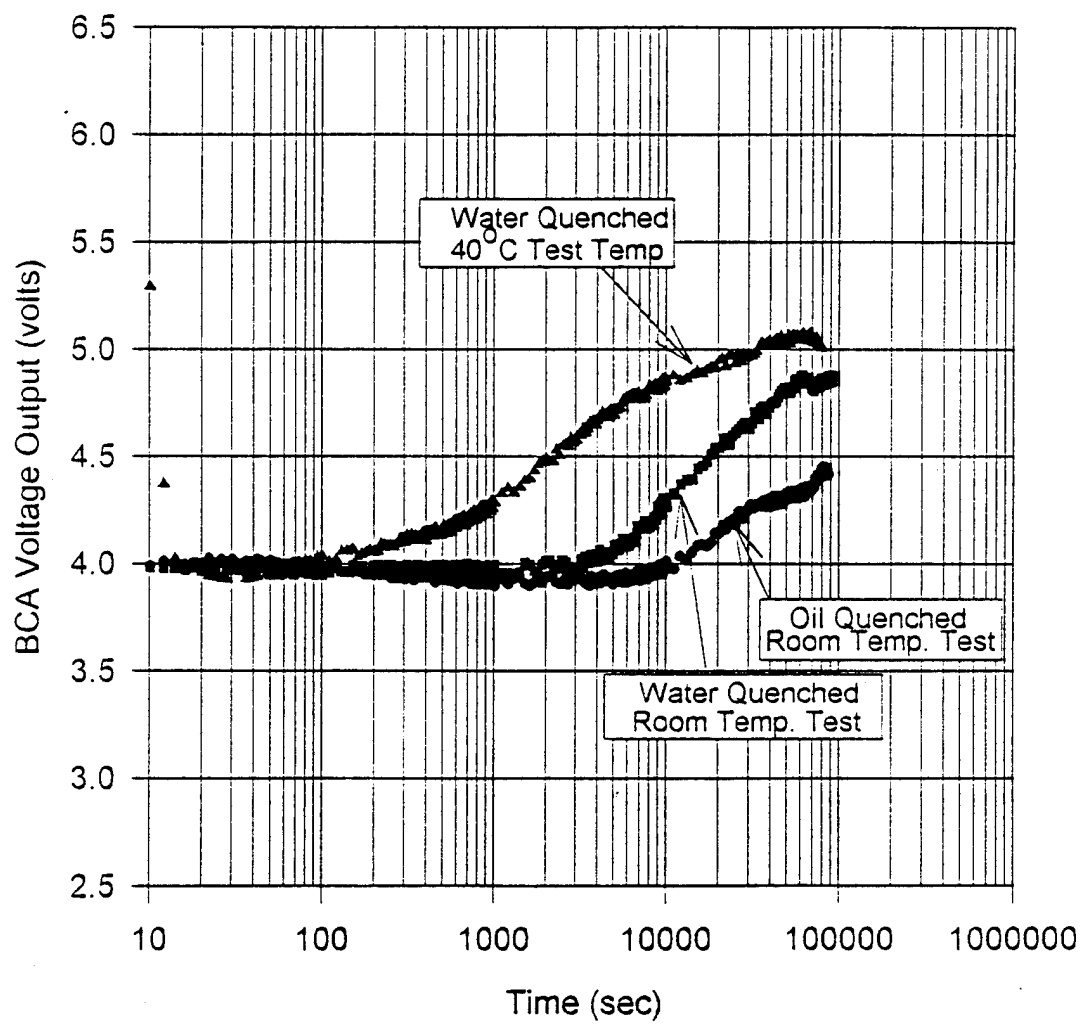Figure 4.5 Yield strength versus aging time for an Al 7075 alloy. From Ref. [15].

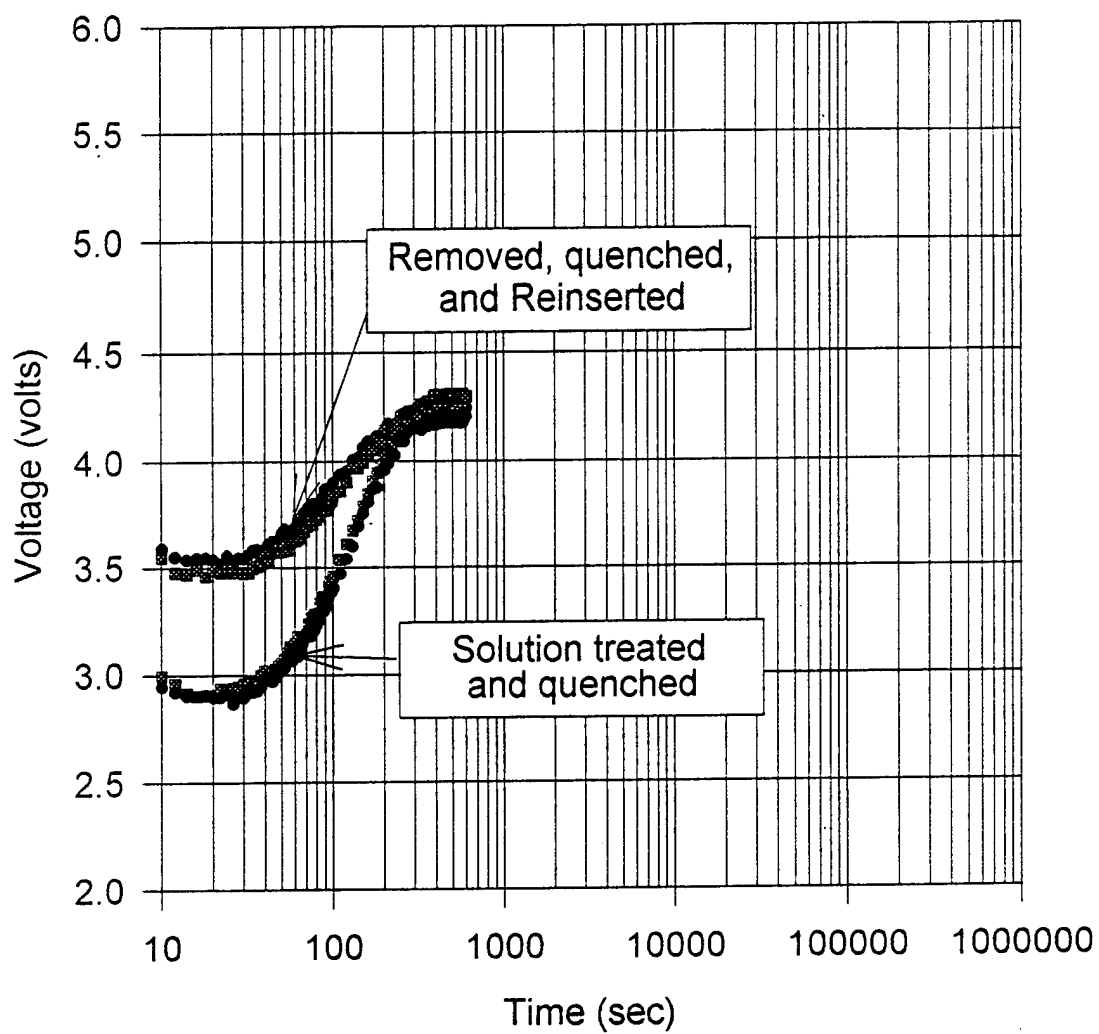**Figure 4.6   BCA voltage versus aging time for three different samples.**

Figure 4.7 Effects of G.P. zone formation on BCA voltage output.

D. STARTING POINT OFFSET

An apparently random variation in the initial BCA voltage was noted throughout the course of more than 100 experiments with this apparatus. In other words, the initial BCA voltage output, at time t = 0, varied from 1.5 V to 3.5 V with apparently identical samples. A series of experiments were conducted to identify the cause(s) of this variation. Factors considered included: (a), the initial state of a given sample; (b), the initial null setting prior to sample insertion; (c), inconsistency of sample placement; and (d), initial temperature differences. The first two factors were deemed responsible for the greatest variation, while the last two are apparently only minor problems.

First, it was established that, with all conditions identical, the BCA output was the same for different samples. This was accomplished by sectioning an as delivered sheet of AL 7075-T6 to produce samples from locations adjacent to one another. When these four adjacent samples were alternately placed in the apparatus (at room temperature) all four samples gave identical BCA voltage outputs (Fig. 4.8). The variation problem arises when such samples are solutionized and subsequently quenched. The fast quench rate required to trap solute atoms and vacancies inevitably creates residual stresses within the sample due to non-uniformity in the cooling rate. These induced stresses produce distortion, or warpage, particularly in thin samples. As shown in Fig. 4.9, two identical samples give the same voltage output in the as-received condition. When subjected to identical solution heat treatment and quenching, the voltage output differs by almost 1.0 volt. Visual examination revealed that sample 2 had distorted to a greater extent during the treatment than did sample 1. Manually bending a sample to differing degrees proved that the voltage increased with increased distortion , as shown in Fig. 4.10(a&b). This was true whether the sample was placed in the apparatus with convex or concave curvatures upward. The cause of the initial voltage variation lies in the standoff resulting from the distortion. The magnitude of the induced eddy currents in a sample depends on the distance between the coils, or source of the field, and the surface of the sample being tested. This dependence is known as a "lift-off" effect and is described in more detail in
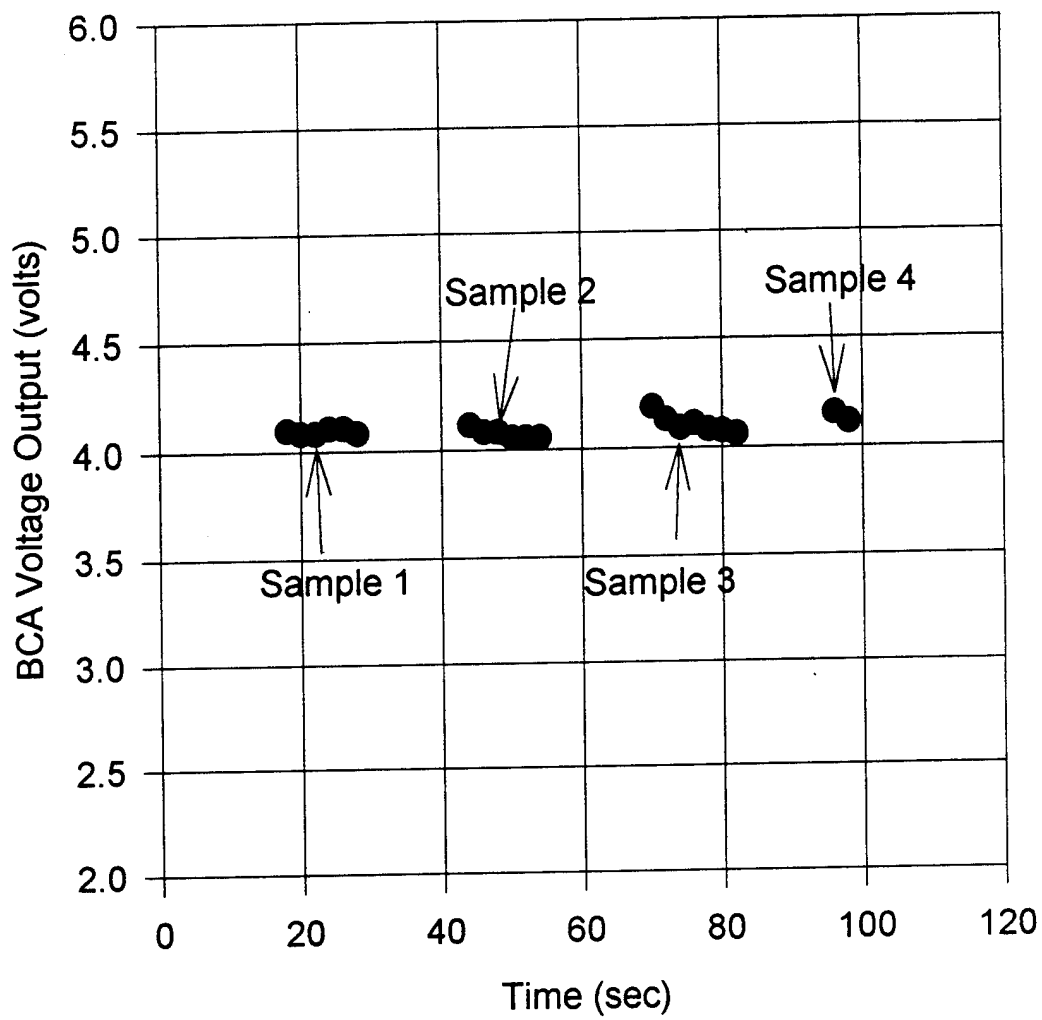
45

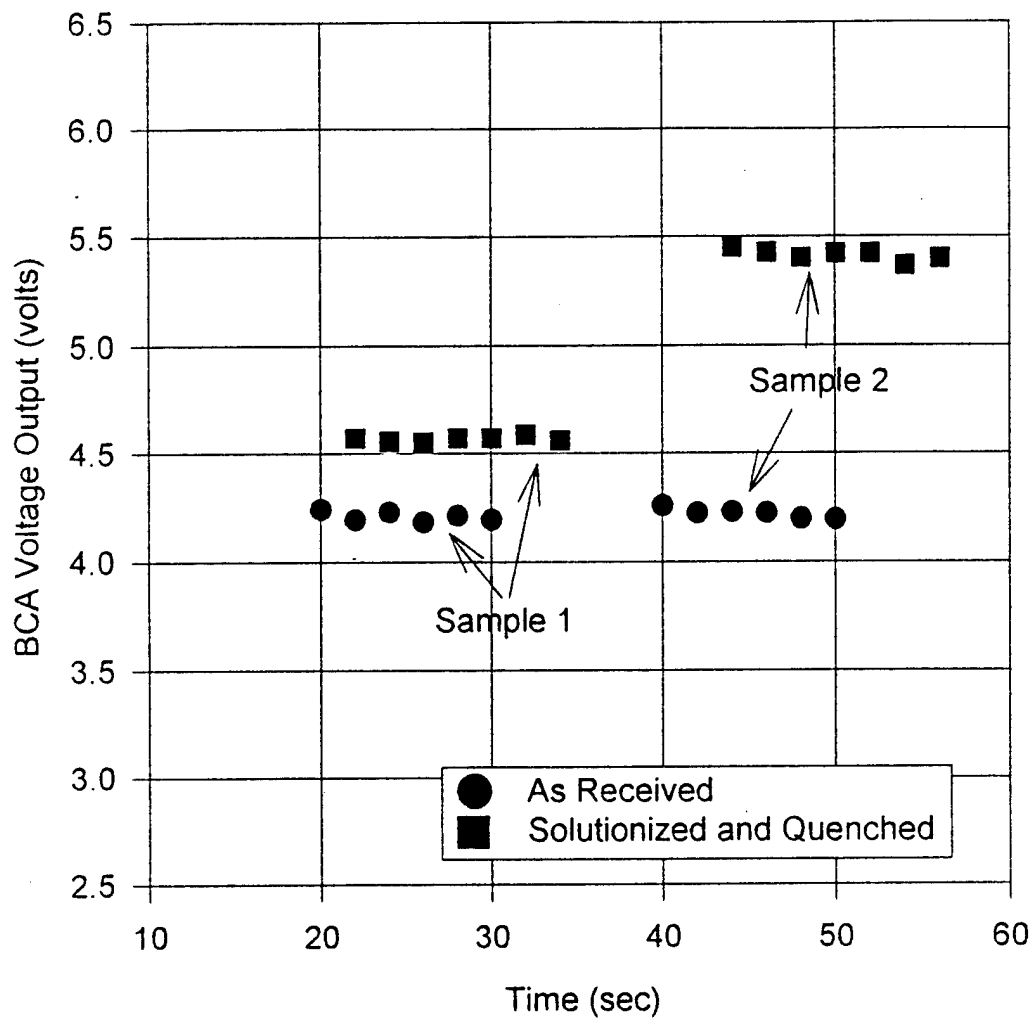**Figure 4.8 Identical BCA voltage output of four as-received samples prior to solution heat treatment and quench.**
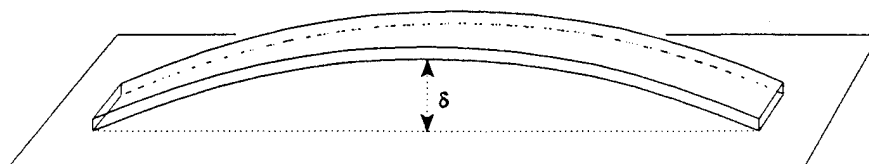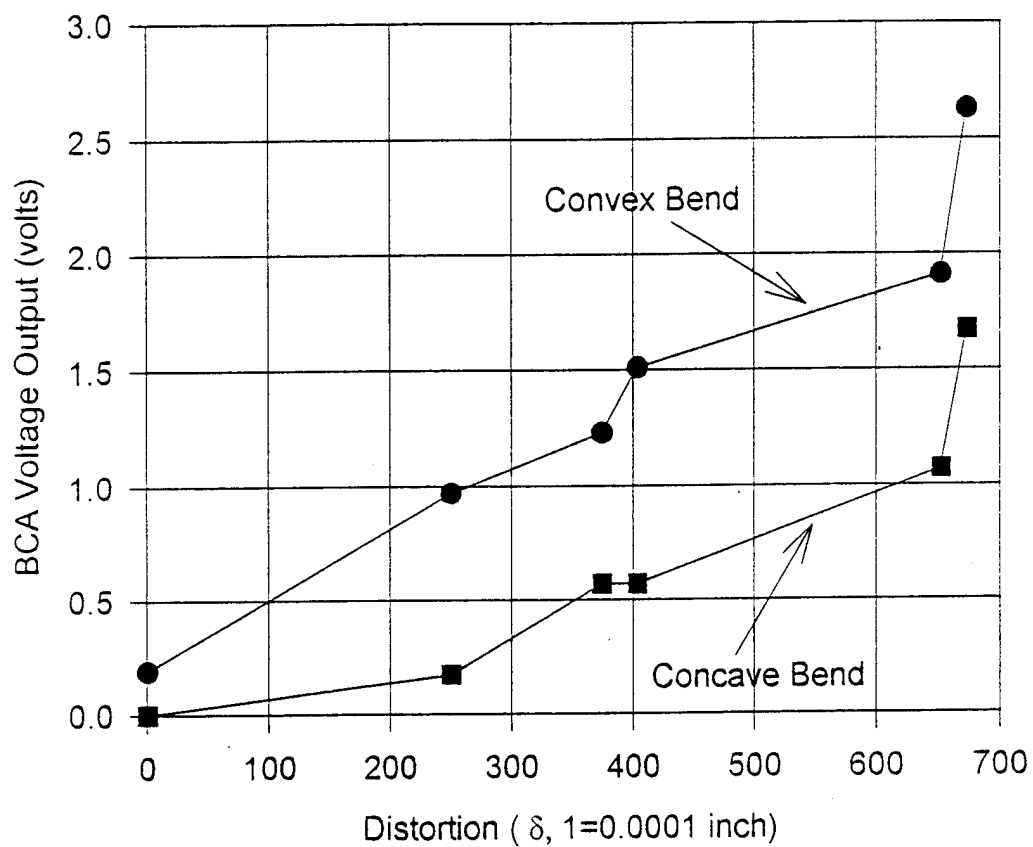
Figure 4.9 Variation in BCA voltage output as a result of distortion caused by rapid quenching.

(a)

Distortion (δ, 1=0.0001 inch)

(b)

Figure 4.10 Increasing voltage as a result of increasing distortion.

48

Chapter 2. Using a micrometer, a sample was incrementally lifted away from the eddy current probe and the resulting voltage output was recorded. Figure 4.11 shows that a standoff as small as 0.003 inches (0.08 mm) is enough to produce an increase in voltage output of about 1.0 volt.

The variation caused by the initial null setting can also be attributed in part to distortion, but in this case the reference sample is the problem. When an experimental run is performed, the BCA voltage output is nulled when the two pure aluminum samples are in thermal equilibrium at the set furnace temperature. If the input voltage varies or either of the two reference samples are distorted the null setting will change. These variations create a change in initial bridge output voltage as can be seen using Eq. 3.1. Changing the initial impedance (Z_1 or Z_2) of either bridge leg creates an initial unbalance which is transferred to the test samples initial voltage output.

Two other minor causes of the initial voltage offset were inconsistent placement and initial temperature differences. Although the apparatus has been designed to give precise lateral placement, there is enough room to create a +/- 0.1 volt variation if the placement is not identical. Additionally, test sample initial temperatures are not always identical because of variations in room temperature at the time of the test. This can create an offset in that a colder sample has a lower resistivity and thus a lower initial BCA voltage. This phenomenon is examined in more detail in the following section. The variations of room temperature during the course of these experiments was minimal so that the changes to initial voltage caused by this were slight.

E. INITIAL TRANSIENT REGION

The initial transient region is the section of the BCA voltage output versus time plots occurring between 0 and about 600 seconds. It is characterized by a slight initial drop followed by a sharp rise which eventually levels off to a peak voltage value. Three phenomena govern behavior during this time interval.
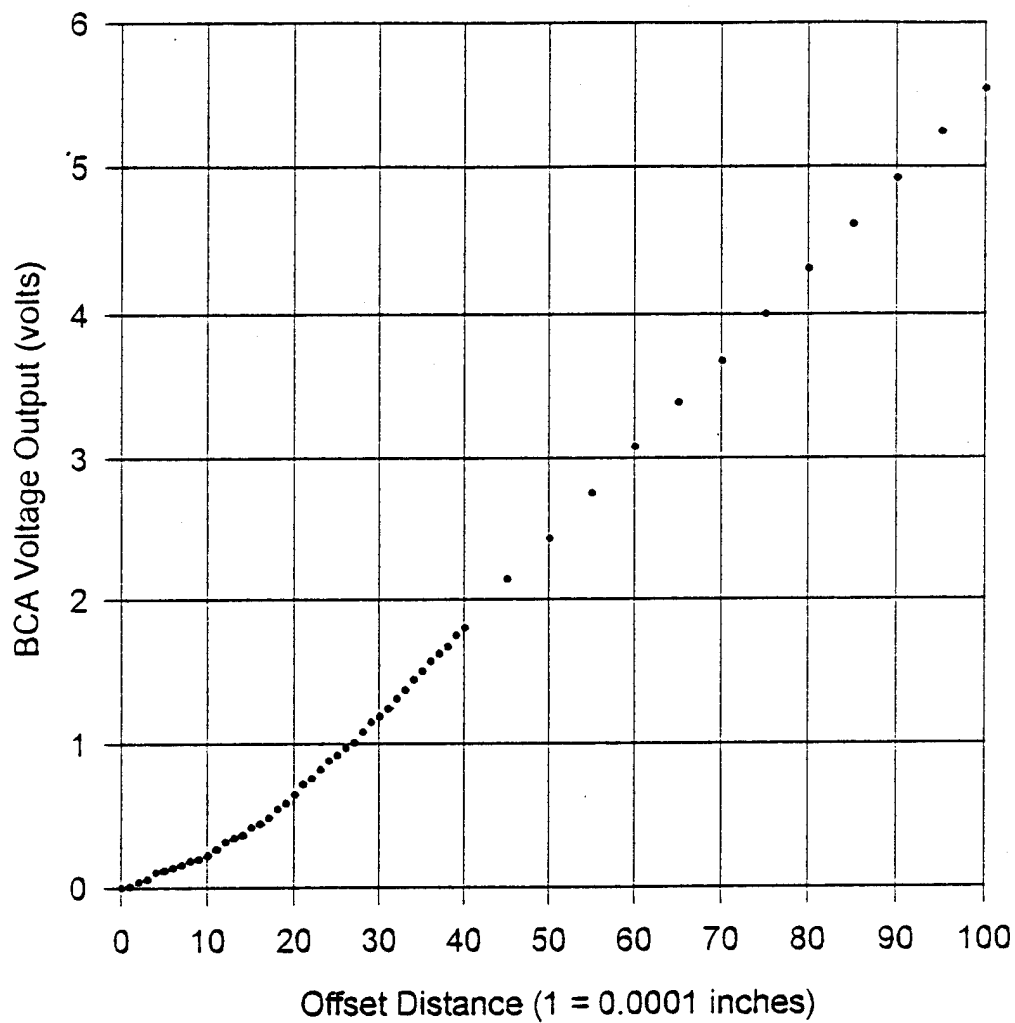
Figure 4.11 Voltage increase as a function of lift-off distance.

First, the test sample, at room temperature, must heat up to the fixed first stage testing temperature. As described in Chapter III, this rise in temperature creates an increase in resistivity, within the material, due to increased thermal vibrations of the atoms. Figure 4.12(a&b) shows the effect initial sample temperature mismatch has on the transient zone. When a sample was quenched in ice water just prior to inserting into the apparatus, the resultant initial transient curve was extended toward a lower initial voltage output. This indicates a lower resistivity in the test sample due to lower sample temperature. The same result can be obtained using a higher test temperature. Three samples of Al 7075-T6, with identical room temperature initial voltage readings, were placed in the apparatus at progressively higher test temperatures. The -T6 temper samples were used so that G.P. formation would not be a factor. Figure 4.13 shows that when the furnace temperature is set higher, the resulting curve becomes elongated, once again in the direction of a lower voltage. This is caused by the higher initial resistivity in the pure aluminum sample at higher temperatures.

Also occurring during this initial transient is the rapid formation of G.P. zones as discussed previously. As the temperature is increased, the formation of G.P. zones is accelerated, as shown in Fig. 4.6. Due to the coherent interface the G.P. zones share with the surrounding matrix, a strain field is developed which increases the resistivity of the material. The resistivity continues to increase as the G.P. zone size increases. Finally a balance is reached when the number of solutes and vacancies in solution is decreased enough to slow down formation of the zones and, at the same time, allow for greater electron mobility throughout the matrix. Figure 4.7 shows the effect of G.P. zones during this initial transient and is described in the preceding section.

During the first minute, while the sample begins to heat up, there is occasionally a small drop off in BCA voltage prior to the rapid increase. There are three possible explanations for this occurrence. First, as the oven door is opened for sample insertion, the temperature of the reference sample drops which lowers its resistance. Secondly, a slight drop in temperature of the probe coils during sample insertion may result in a drop
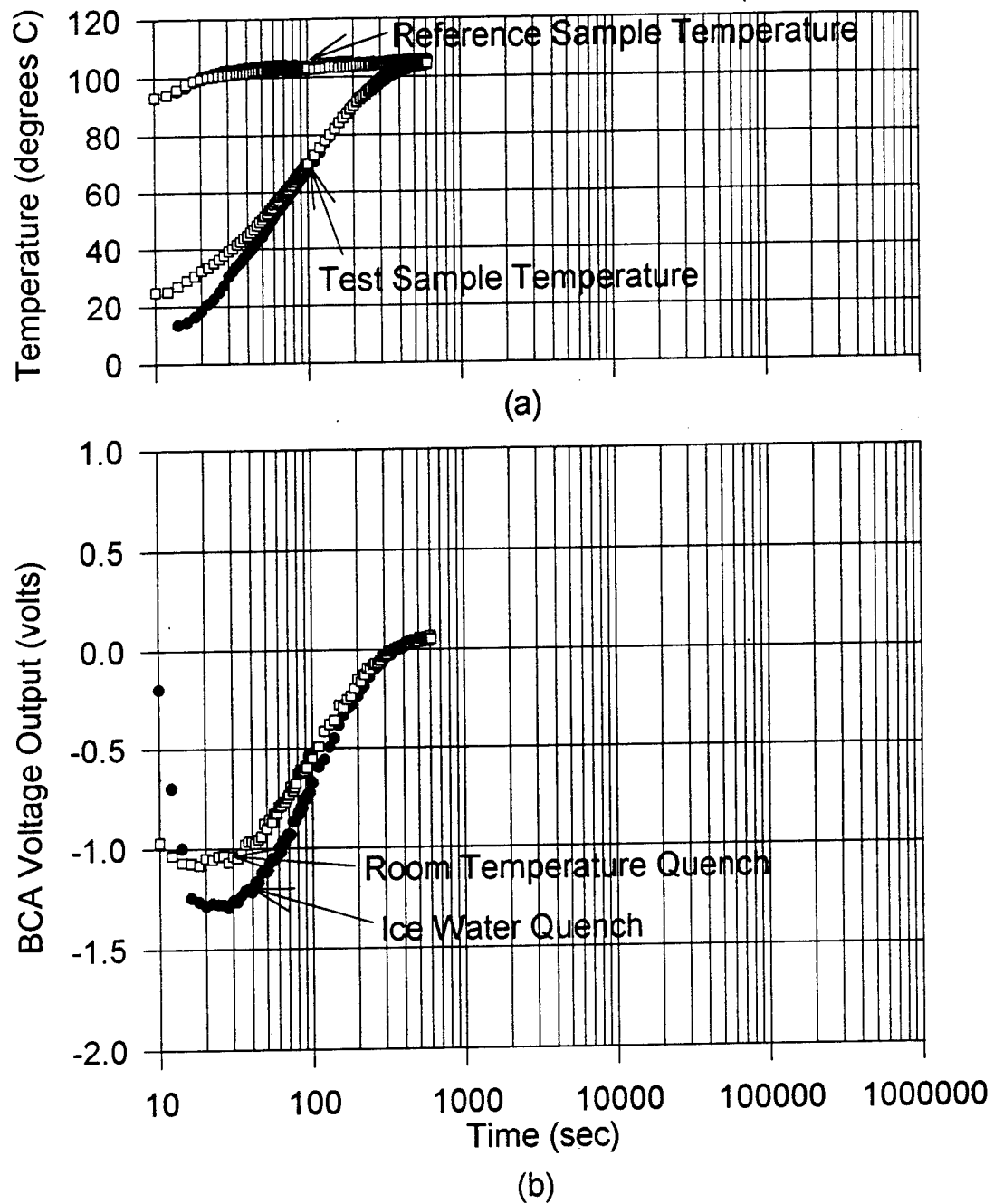
Figure 4.12 Variation in transient region as a function of sample temperature. (a) Temperature difference between test and reference samples. (b) Elongation of the initial transient curve due to lower temperature sample.
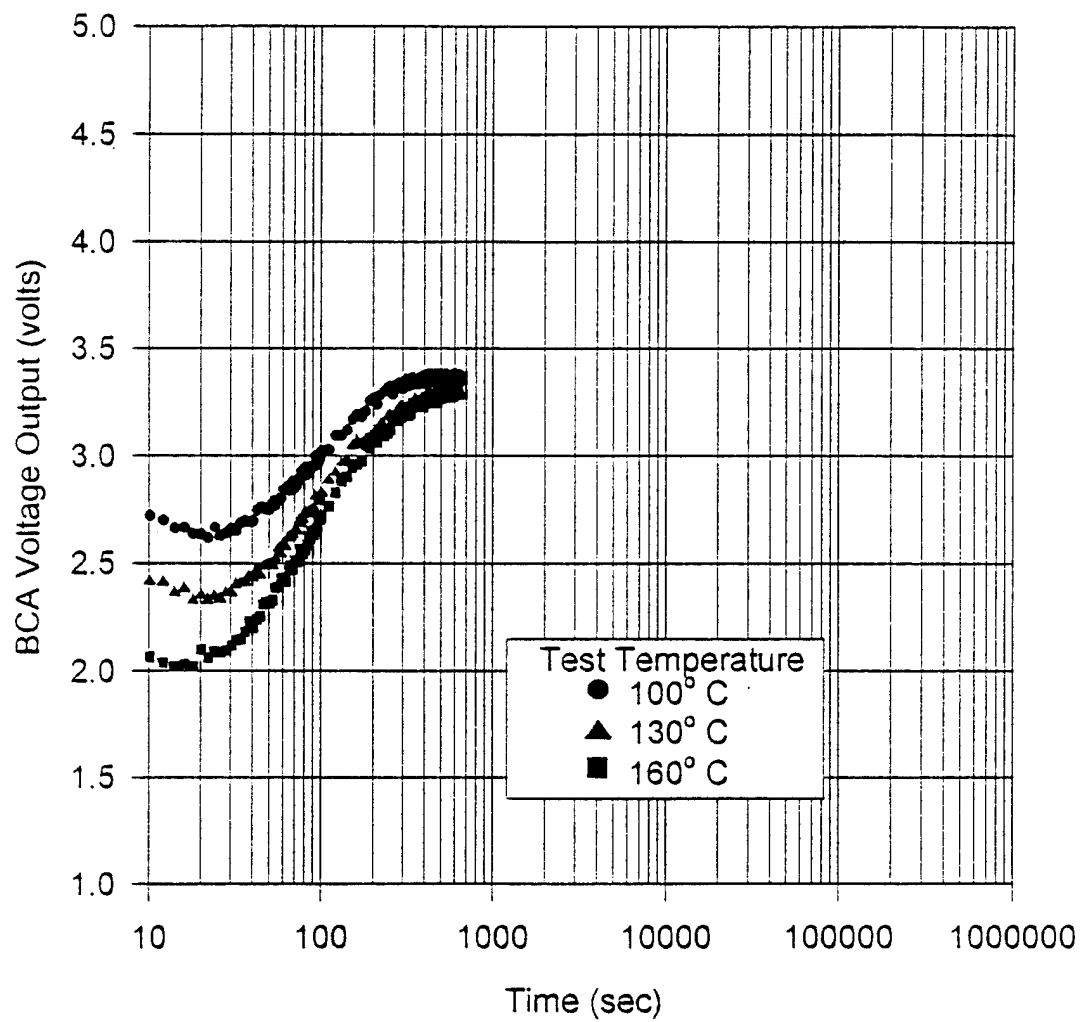
Figure 4.13 Variation in transient region as a function of oven temperature.

in BCA output. Finally, as the sample begins to heat up, extremely small G.P. zones, may undergo what is termed reversion [Ref. 10]. These smallest zones begin to nucleate as soon as the material is quenched in an attempt to lower the high free energy associated with the trapped in vacancies and solutes. Since these initial zones are not of sufficient size to be stable at higher temperatures, they dissolve back into the matrix. This relieves the strain fields associated with the zones and thus lowers the resistivity. Eventually, as the temperature continues to increase, new nuclei are able to form.

F. TRANSIENTS DURING STEP CHANGES IN TEMPERATURE

A second transient occurs when there is a step change in temperature during a multi-stage heat treatment operation. This region covers the section of curve just prior to the temperature increase up until the two samples are again in thermal equilibrium with the furnace. In each multi-stage experiment conducted, the second transient included a sharp drop in BCA voltage. Matthiessen's rule (Eq. 2.3) states that the resistivity increases in the pure aluminum reference sample and the aluminum alloy should be essentially identical and no change of output voltage should occur. This would be true as long as the two samples have identical thermal coefficients of resistivity and the resistivity contribution of lattice defects, ρ_i , is not a function of temperature.

The thermal coefficient of pure aluminum at 20° C is given as 114.5×10^{-12} ohm-m/K while for Al 7075 the value of the coefficient is 100×10^{-12} ohm-m/K [Ref. 5]. Thus, when the temperature is increased to the second-stage temperature the pure aluminum resistivity would increase more than that of the Al 7075 test sample, assuming these values could be extrapolated to higher temperatures. Thus, an overall drop in BCA output voltage will be obtained. Conducting a test with an overaged sample, at lower temperatures, revealed similar voltage drops.

In the case of a hardenable alloy, increasing the temperatures allows the solutes to diffuse out of the matrix more quickly to join the already developed intermediate phase precipitates. Fewer solutes in solution increases the electron mobility and decreases the

overall resistance. While the resistivity in both samples is increasing, due to the increased temperature, the test sample increase is reduced due to the negative effect of an increased precipitation rate. Figure 4.14 shows a two-stage heat treatment process to achieve the -T6 condition in an initially solutionized Al 7075 sample. Figure 4.15 shows an expanded view of the second transient zone. At the end of the transient there is an apparent overshoot of the BCA voltage and ensuing recovery prior to the subsequent decrease; this is caused by the lag of the test sample in reaching thermal equilibrium. This lag is due to the lower thermal conductivity of the alloy compared to the control sample. As the temperature of the test sample begins to catch up to the reference sample, the resistivity of the alloy continues to increase while that of the pure aluminum is beginning to level off. Thus the voltage output starts to increase accordingly until it reaches its equilibrium value.

G. MONITORING CONCEPT

A clear pattern was observed throughout the multitude of single and multi-stage heat treatments performed in this work. Although the voltage values varied for nominally identical tests, nearly identical voltage-time curves resulted when the data were normalized to a common peak value as seen in Fig. 4.2. The single-stage heat treatment was characterized by an initial transient followed by a slow decrease in voltage as the test progressed. The slow decline in BCA output is the result of the decrease in resistivity of the Al 7075 test sample due to the continued growth of the intermediate precipitates.

Multi-stage heat treatments also displayed an initial transient followed by a slow decrease in voltage. The slope of this portion was less steep than that of a single-stage treatment because of the reduced temperature of the first stage. When the temperature was subsequently increased to that of the second stage, a pronounced transient drop in voltage was observed for reasons outlined in the preceding section. Following this rapid drop, the voltage output once again gradually declined now at a greater rate than the first stage due to the increased diffusivity of solute atoms at this higher temperature. A multi-stage heat treatment of an Al 2024 [Fig. 4.16], using the same process recommended for

Al 7075 [Ref. 15], revealed a lesser rate of change during the second stage. This is a result of the higher heat treatment temperature, 190° C versus 163° C, required for Al 2024. These data indicate wide potential applicability for such a technique in the heat treatment of many age-hardenable materials.
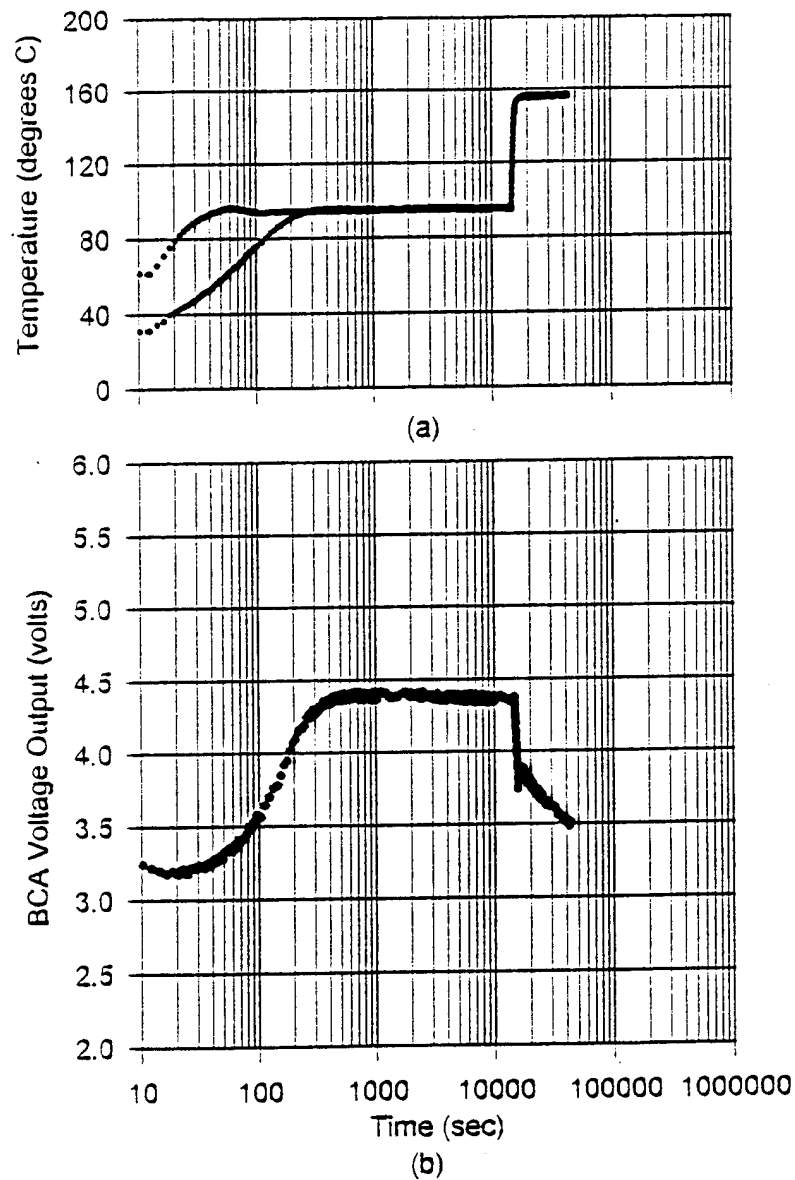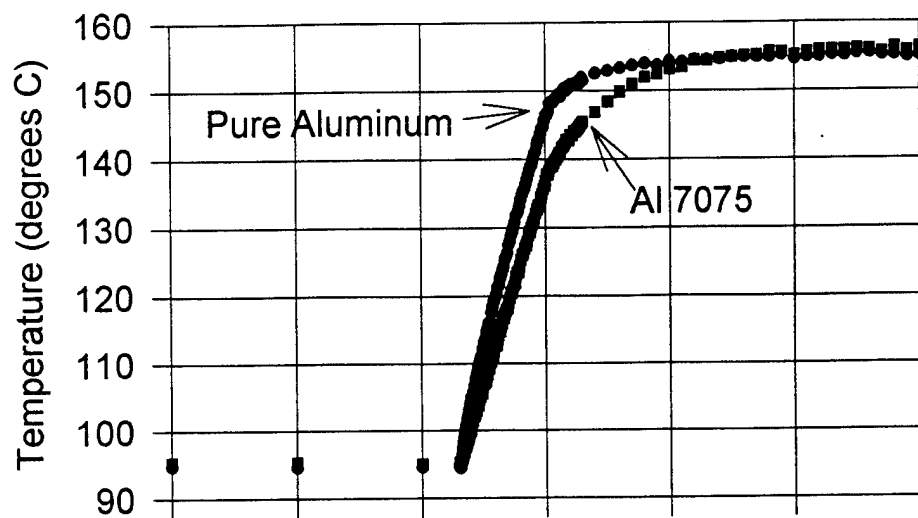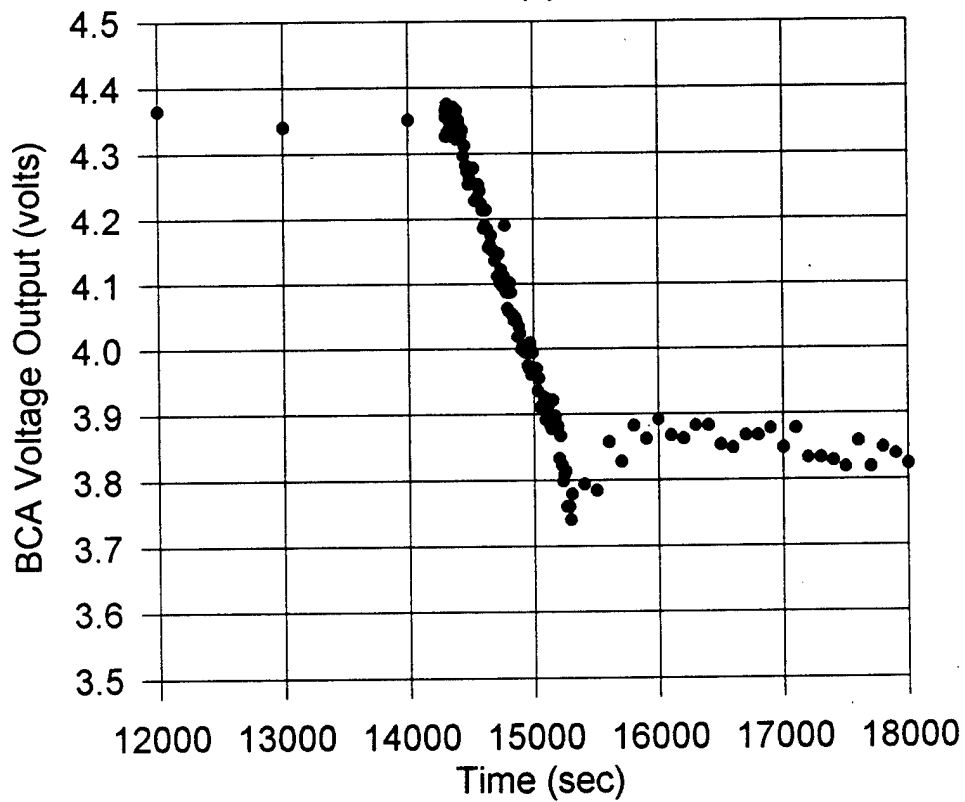

Figure 4.14 Two-stage heat treatment to achieve a -T6 condition in Al 7075.

Figure 4.15 Expanded view of the step increase in temperature to the second stage heat treatment.
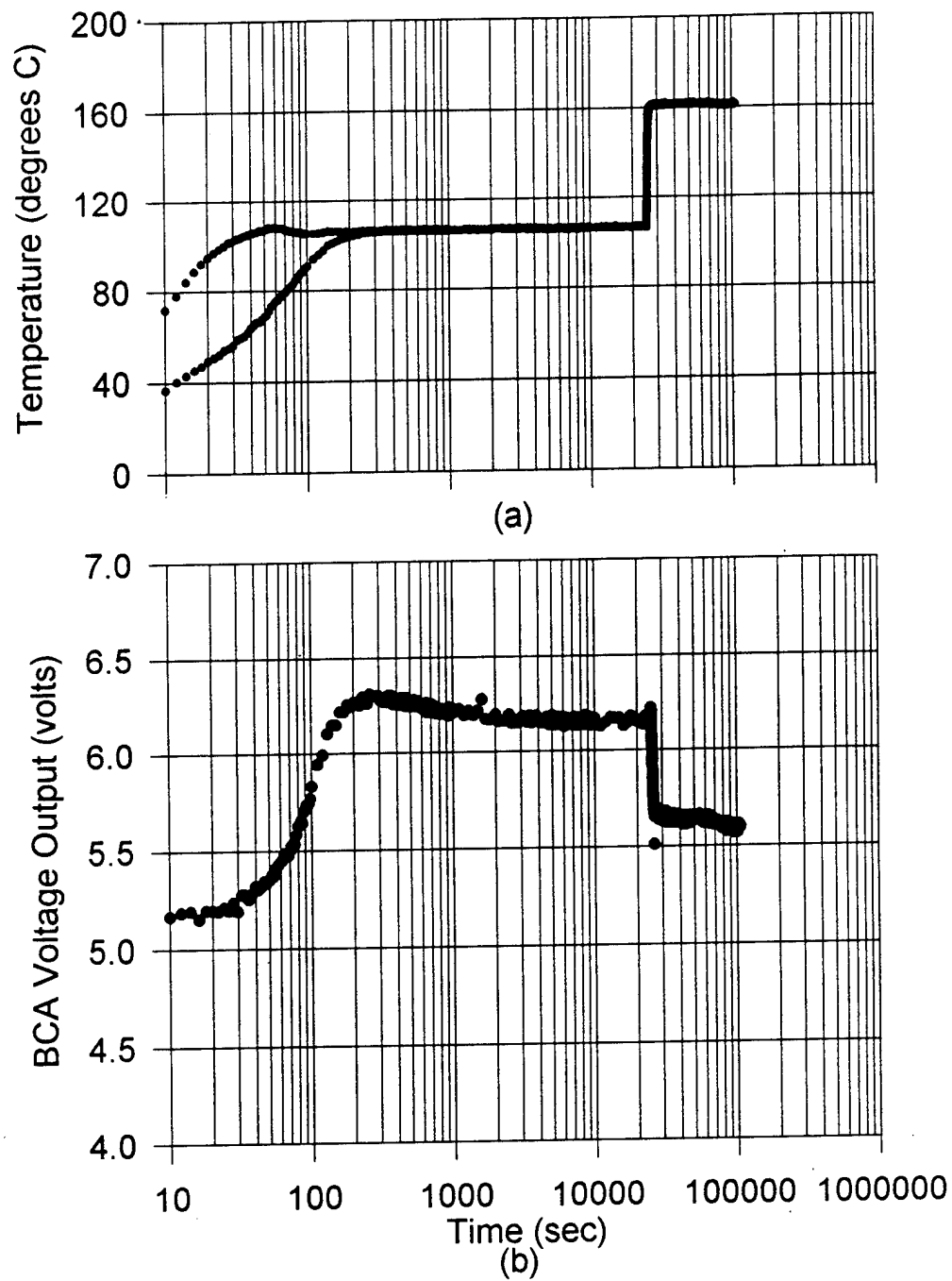
Figure 4.16   Two-stage heat treatment of an Al 2024 sample.

V. CONCLUSIONS AND RECOMMENDATIONS

The following conclusions and recommendations were drawn as a result of this thesis project.

A. CONCLUSIONS

1. System Calibration

With two identical pure aluminum specimens in the apparatus there is a reproducible BCA voltage versus temperature relationship. The observed increase in voltage with temperature is a function of the mismatch between the two eddy current probe coils. The hand wound coils may have been constructed with a different number of turns on each, variable spacing between the turns or inconsistent tension. Any of these discrepancies would create a change in voltage due to thermal expansion of the coiled wires.

2. G.P. Zone Formation

The system was able to monitor the increasing resistivity of a solutionized sample during ambient temperature aging at times that correspond to the onset of increase in yield and tensile strengths for aging of the same alloy type in the same solutionized condition. A slower quench rate produced a delay in the increase in resistivity, i.e. the onset of G.P. formation, due to vacancy diffusion during the quench. By increasing the testing temperature, the time before the resistivity increased was reduced. This acceleration is caused by the increased diffusion rate at a higher temperature.

3. Variation in Initial Voltage BCA Readings

Although the shapes of the BCA voltage versus time plots were virtually identical for replicate tests, variations of the starting voltage was observed by as much as 1.5 to 2.0

volts. This is the result of three factors. Initial null setting varied due to distortion of the pure aluminum reference sample; distortion of the test sample during quenching; and inconsistencies in sample positioning in the apparatus. The first two factors had the biggest effect.

4. Initial Transient Region

The initial transient region (0 to 600 sec.), where a rapid change in resistivity is observed, may be attributed to thermal equilibration and, simultaneously, to the formation of G.P. zones as the temperature increased. Increased thermal vibration of the atoms caused by the temperature increase, coupled with the strain fields produced around the G.P. zones, work simultaneously to increase the resistivity of the alloy.

5. Transient During Step Change in Temperature

Transients in the multi-stage heat treating consisted of sharp drops in voltage as the reference and test samples reached equilibrium after heating from one temperature to another. Matthiessen's rule states that the resistivity increase in the pure aluminum and the aluminum alloy should have been identical and no change should have occurred. This rule, however, does not take into account the accelerated formation of precipitates in the alloy. Also, although the resistivity of the alloy is increasing, it is likely increasing at a lower rate than that of pure aluminum.

6. Monitoring Concept

The single-stage heat treatment was characterized by the initial transient curve followed by a slow decrease in voltage as the test progressed. The multi-stage heat treatment followed the same initial transient curve but had a slower decrease during the first stage due to a lower temperature. When the temperature was increased for the second stage of the heat treating process, the voltage initially showed a rapid drop followed by a rate of decrease greater than that of the first stage. Although the starting

point varied from test to test by as much as 1.5 to 2.0 volts, when normalized to the peak voltage, the curves overlapped. Such voltage-time relationships may be used to provide feed back to a control system in order to achieve more precise control of heat treatment processes.

B. RECOMMENDATIONS

Further investigation of the correlation between BCA voltage output and mechanical properties should be conducted. These data could be used in the programming of a control system for an actual heat treatment operation

The apparatus must be redesigned so that reproducible placement of the coil on the sample is achieved to reduce the effects of lift-off. Using shorter or thicker samples may reduce the distortion during the quench enough to proceed testing with the current apparatus. This, however, may limit the type of mechanical testing to hardness alone.

An investigation into the possibility of converting this eddy current system into a scientific device to study precipitation effects should be conducted. The comparability of the BCA output to known physical occurrences during various tests indicate that this system may be a useful laboratory tool.

The probe coils should be professionally constructed to be as identical as practicable in order to offset the variation in system response with increased temperature. Additionally, coils of various sizes should be made so that a range of test frequencies and depths of penetration could be examined.

LIST OF REFERENCES

1. Esarey, John G., *Continuous Measurement By Eddy Current Methods of Age Hardening in Aluminum Alloys*, Master's Thesis, Naval Postgraduate School, Monterey, California, September, 1992.

2. Mata, Silvester G., *Continuous Measurement of Aging Response in Aluminum Alloys By Eddy Current Methods*, Master's Thesis, Naval Postgraduate School, Monterey, California, December, 1993.

3. Persampieri, D., San Roman, A., Hilton, P., "Process Modeling for Improved Heat Treating", *Advanced Materials and Processes*, v.139, pp. 19-23, March 1991.

4. Rossiter, P.L., *The Electrical Resistivity of Metals and Alloys*, Cambridge University Press, 1987.

5. *Metals Handbook*, 9th Edition, Vol. 2, edited by Baker, H., et. al., American Society for Metals International, 1979.

6. Smallman, R.E., *Modern Physical Metallurgy*, Butterworth & Co. Ltd, 1985.

7. Callister, W.D., *Material Science and Engineering, An Introduction*, 2nd Edition, John Wiley & Sons, Inc., 1991.

8. *Metals Handbook*, 9th Edition, Vol. 17, edited by Lampman, S.R., et. al., American Society for Metals International, 1989.

9. Halliday, D., Resnick, R., *Fundamentals of Physics*, Extended 3rd Edition, John Wiley & Sons, Inc., 1988.

10. Martin, J.W., *Precipitation Hardening*, Pergamon Press Ltd., 1968.

11. Seltzer, D.D., *Correlation of Conductivity to Mechanical Properties of Age-Hardenable Aluminum Alloys Using Eddy Current Methods*, Paper from the "Proceedings for the Fifth International Conference on Non-Destructive Testing", Department of Energy, Mines and Resources, 1969, pp.283-291.

12. Rosen, M., Horowitz, E., Swartzendruber, L., Fick, S., Mehrabian, R., "The Aging Process in Aluminum Alloy 2024 Studied by Means of Eddy Currents", *Materials Science and Engineering*, v. 53, pp. 191-198, 1982.

13. Rummel, W.D., Arbegast, W.J., *Characterization of 2014, 2219, 6061, and 7075 Aluminum Alloy Heat Treatment Response by Eddy Current Conductivity, Hardness and Mechanical Properties*, American Society for Non-Destructive Testing, Inc., 1980.

14. Rosen, M., "Eddy Current Analysis of Precipitation Kinetics in Aluminum Alloys", *Metallurgical Transactions A*, v.20A, pp. 605-610, April 1989.

15. *Metals Handbook*, Vol. 4, edited by Lampman, S.R., et. al., American Society for Metals International, 1991.

16. Hatch, J.E., *Aluminum: Properties and Physical Metallurgy*, American Society for Metals, 1984.

17. Private communication between Tom Christian, Electronic Instrument Support, Code 34 and Robert Hall, 10 January, 1995.

INITIAL DISTRIBUTION LIST

1. Defense Technical Information Center   2
   Cameron Station
   Alexandria, VA 22304-6145

2. Library, Code 52   2
   Naval Postgraduate School
   Monterey, CA 93943-5101

3. Chairman, Code ME   1
   Mechanical Engineering Department
   Naval Postgraduate School
   700 Dyer Rd., Rm. 328
   Monterey, CA 93943-5100

4. Dr. Terry R. McNelley, Code ME/MC   5
   Mechanical Engineering Department
   Naval Postgraduate School
   700 Dyer Rd., Rm 328
   Monterey, CA 93943-5100

5. Naval/Mechanical Engineering Curricular Office, Code 34   1
   Naval Postgraduate School
   700 Dyer Rd., Rm. 115
   Monterey, CA 93943-5100

6. Dr. William Frazier, Code 6063   2
   Naval Air Warfare Center
   Warminster, PA 18974

7. Robert A. Hall Jr.   2
   c/o Mary E. Havey
   20 Peter St.
   Orono, ME 04473